THE BAIA – FONDI DI BAIA ERUPTION AT CAMPI FLEGREI: STRATIGRAPHY AND DYNAMICS OF A MULTI-STAGE CALDERA REACTIVATION EVENT

Marco Pistolesi[1*], Antonella Bertagnini[2], Alessio Di Roberto[2], Roberto Isaia[3], Alessandro Vona[4], Raffaello Cioni[1], Guido Giordano[4]

[1] Dipartimento di Scienze della Terra, Università di Firenze (Italy)
[2] Istituto Nazionale di Geofisica e Vulcanologia, Sezione di Pisa (Italy)
[3] Istituto Nazionale di Geofisica e Vulcanologia, Osservatorio Vesuviano, Napoli (Italy)
[4] Dipartimento di Scienze, Università di Roma Tre (Italy)

*corresponding author:
Dipartimento di Scienze della Terra, Università di Firenze, via La Pira, 4, 50121, Florence, Italy
Tel. +390552757574 / +390552757479
Email : marco.pistolesi@unifi.it

Keywords: Campi Flegrei, stratigraphy, tephra deposits, eruptive dynamics, caldera.

Abstract

The Baia – Fondi di Baia eruption is one of the sporadic events that have occurred in the western sector of the Campi Flegrei caldera. It dates back to 9525–9696 BP, and opened Epoch 2 of the caldera activity after a 1000 year-long period of quiescence. Although relatively small in terms of erupted volume with respect to most of the events of the past 15 ka, the Baia – Fondi di Baia eruption was characterized by a complex series of events, which have led to different interpretations in the literature. We present a detailed stratigraphic study of 40 outcrops in a sector of about 90 km^2, coupled with sedimentological (grain-size, componentry), physical (density, vesicularity), textural, and compositional analyses of the erupted deposits. Based on these data, we interpret the stratigraphic succession as being related to two distinct eruptive episodes (Baia and Fondi di Baia). These were separated by a short time interval, and each was characterized by different eruptive phases. The Baia eruptive episode started in a shallow-water environment with an explosive vent-opening phase that formed a breccia deposit (Unit I), rapidly followed by alternating fallout activity and dense, pyroclastic density current deposits generation (Unit II). Sedimentological features and pumice textural analyses suggest that deposition of Unit II coincided with the intensity peak of the eruption, with the fallout deposit being characterized by a volume of 0.06±0.008 km^3 (corresponding to a total erupted mass of $4.06 \pm 0.5 \times 10^{10}$ kg), a column height of 17 km and a corresponding mass flow rate of 1.8×10^7 kg s^{-1}. The associated tephra also shows the highest vesicularity (up to 81 vol.%), the highest vesicle number density (1.01×10^8 cm^{-3}) and decompression rate (0.69 MPa s^{-1}). This peak phase waned to turbulent, surge-like activity possibly associated with Vulcanian explosions and characterized by progressively lower intensity, as shown by density/vesicularity and textural properties of the erupted juvenile material (Unit III). This first eruptive episode was followed by a short quiescence, interrupted by the onset of a second eruptive episode (Fondi di Baia) whose vent opening deposited a breccia bed (Unit IV) which at some key outcrops directly overlies the fallout deposit of Unit II. The final phase of the Fondi di Baia episode strongly resembles Unit II, although sedimentological (presence of obsidian clasts which are absent in the Baia deposits), and textural (lower vesicularity, vesicle number density and decompression rate values) features, together with a more limited dispersal, suggest that this phase of the eruption had a lower intensity. The large range of groundmass glass compositions, associated with variable proportions of highly (phonolitic-trachytic) and mildly (tephriphonolitic-latitic) evolved end-members in the products erupted during the two episodes, also suggests that these eruptive episodes were fed by at least two different magma batches that interacted during the different phases, with an increase of tephriphonolitic-latitic magma occurring during the Fondi di Baia stage.

1. Introduction

The Campi Flegrei caldera (CFc) is located in Southern Italy, in the western part of the densely populated (~1.5 million people) area of the Bay of Naples. The caldera is the result of two main eruptive events, the Campanian Ignimbrite (CI, 39.8 ka BP, Giaccio et al. 2017) which erupted at least 200 km^3 of trachytic to phono-trachytic magma (e.g. Civetta et al. 1997; Smith et al. 2016), and the Neapolitan Yellow Tuff (NYT, 15 ka BP, Deino et al. 2004) which was characterized by the emplacement of 40 km^3 of latitic to trachytic magma (Orsi et al. 1992, 1995; Scarpati et al. 1993; Wohletz et al. 1995). The eruptions of the post-NYT period were confined within the structural boundaries of the caldera and comprised at least 70 known events (Di Renzo et al. 2011), dominated by low- to medium-magnitude phreatomagmatic-magmatic eruptions with volumes of <0.1 km^3 (Di Renzo et al. 2011; Orsi et al. 1995; Smith et al. 2011). The 70 post-NYT eruptions are grouped into three eruptive epochs, separated by periods of quiescence: Epoch 1 (15.0–10.6 ka BP), Epoch 2 (9.6–9.1 ka BP), and Epoch 3 (5.5–3.5 ka BP) (Di Vito et al. 1999; Isaia et al. 2009, Smith et al. 2011). The most recent event was the Monte Nuovo eruption of 1538 AD (Guidoboni and Ciuccarelli, 2011; D'Oriano et al. 2005). Positions of eruptive vents vary through the three epochs (Bevilacqua et al. 2015). During Epoch 1 vents were mainly aligned along the structural boundaries of the NYT caldera, but Epoch 2 was mainly characterized by eruptions from the NE sector of the caldera, with the exception of the Baia – Fondi di Baia eruption. This occurred at onset of Epoch 2 and was located in the western sector of the NYT caldera. Finally, Epoch 3 vents were hosted mainly in the central-eastern sector of the caldera, at the western margin of the Agnano collapse area (Isaia et al. 2009). This area was also affected by the manifestations of unrest during the crises of 1970-1972 and 1982-1984; events which were accompanied by seismicity, increase in heat fluxes and fumarolic activity linked to ground uplift of 3.5 m centred in the Pozzuoli area (Barberi et al. 1984, 1989). The occurrence of continued fumarolic activity, widespread manifestations of hydrothermal springs and ongoing ground deformation suggest that the CFc magmatic system remains in a state of unrest (Vilardo et al. 2010; Chiodini et al. 2012, 2015, 2016).

The Baia – Fondi di Baia eruption consisted of two small-scale eruptive episodes that marked the onset of Epoch 2. They occurred after a 1000-year-long period of quiescence and have been dated to 9525–9696 BP (Di Vito et al. 1999; Smith et al. 2011). The two episodes are representative of the rather sporadic eruptions that have occurred in the western sector of the CFc (Rosi and Sbrana 1987; Di Vito et al. 1999; Orsi et al. 2004; Bevilacqua et al. 2015). Although small in magnitude, the Baia – Fondi di Baia eruption emplaced a complex pyroclastic sequence that has led to contrasting interpretations, with the event being considered as the result of a single eruption (Di Vito et al. 1999; Orsi et al. 2004; Smith et al. 2011), as a sequence of time-separated eruptive events (Rosi and Sbrana 1987), or as two different eruptions (Di Renzo et al. 2011; Bevilacqua et al. 2015). According to Rosi and Sbrana (1987), tephra deposits are the result of the coeval eruption of Baia and Fondi di Baia. They overlie a humified paleosoil, which Rosi and Sbrana (1987) used as a marker horizon to separate the eruptive products in the proximal area of the NYT caldera from those of older eruptions (35,000–11,500 BP). More recently, following the division of the post-15 ka eruptions into three Epochs, the eruption was considered as a single event (Fondi di Baia eruption; Di Vito et al. 1999; Orsi et al. 2004; Smith et al. 2011) or as being two separate events (Di Renzo et al. 2011; Bevilacqua et al. 2015). However, no further detailed stratigraphic investigations have shed light on the source, chronology, activity and deposits of this important event that marked the reactivation of CFc after a long period of quiescence.

Here we present a new stratigraphic study of the entire eruptive succession based on observations of 40 outcrops in and around the Campi Flegrei caldera. Two key sections are described in order to reconstruct the whole stratigraphic record. Description of the tephra architecture is accompanied by sedimentological characterization of the deposits. Physical parameters, including dispersal, volume, column height, total grain-size distribution, are also provided. Juvenile material is also characterized in terms of density/vesicularity, detailed textural analyses, and composition of whole rock and groundmass glasses. Together, our results allow us to make a complete reconstruction of the eruptive sequence and associated dynamics that characterized the Baia – Fondi di Baia eruption.

2. Methods

During stratigraphic and sampling surveys, we investigated 40 outcrops in a sector of about 90 km^2, from proximal (along the crater rims) to distal (30 km farther north of the vent) areas, to define the architecture of the tephra succession (Fig. 1). At each site, the stratigraphy and the textural characteristics of each tephra layers were described in detail. The tephra succession was correlated among the different outcrops mainly based on sedimentological features (color, grain-size, depositional structures). Several key sections located close to the Baia harbour and the Baia castle were particularly useful in tracing correlations between different tephra layers and in reconstructing an “ideal” stratigraphic succession that comprises both products emplaced during the Baia episode and those erupted during the Fondi di Baia episode. Field thickness data (40 thickness measurements) of the fallout phase (lower part of

Unit II) were hand-contoured to produce isopach maps (six contour lines, from 5 to 100 cm). These were used to derive the erupted volume using several fitting methods including one (Pyle 1989) and two (Fierstein and Nathenson 1992) segments on a plot of log thickness vs. square root of the isopach area, and the power law and Weibull fits (Bonadonna and Houghton 2005; Bonadonna and Costa 2013). Tephra fallout volume was then converted to dense rock equivalent (DRE) volume based on assumed bulk density of 2,400 kg m^{-3} and mean deposit density of 700±200 kg m^{-3} (as derived from direct measurements of the deposit in proximal and distal outcrops). An average volume for proximal deposits of pyroclastic density currents (PDCs) was estimated according to the method of Crandell (1989) by integrating the dispersal area with a mean thickness to describe the entire area of deposition. At nine sections, maximum dimensions of lithic clasts were also measured and used to compile isopleth maps. At each section, an area of 0.5 m^2 was investigated. We derived the geometric mean of the three axes of the 20 largest clasts; measures were then combined for the 5 largest clasts and for the 50th percentile of the distribution following Bonadonna et al. (2013). Crosswind and downwind distances were used to derive column heights following the Carey and Sparks (1986) model. Column height was converted to mass/volumetric flow rate by using the relationship of Mastin et al. (2009) and a DRE of 2,500 kg m^{-3} (as required by the strategy suggested by Mastin et al. (2009)). The fallout phase was also classified with the currently used schemes based on erupted volume and mass (Newhall and Self 1982), mass flow rate and plume height (Pyle 2000; Bonadonna and Costa 2013), thinning trend and grain-size data of the deposit (i.e. bc/bt ratio, with bt and bc being the distance over which the maximum thickness and the size of the largest clast decrease by half, respectively) (Pyle 1989). The total grain-size distribution of the fallout phase of Unit II was determined based on the Voronoi tessellation strategy as proposed by Bonadonna and Houghton (2005). In order to close the outermost Voronoi cells located on the edge of the deposit, a zero-mass line was tentatively traced according to field observations and taking into account the position of the outermost isopach contour of the corresponding tephra succession. The Voronoi tessellation was then applied using a *MatLab*® script which returns a probability density function for the total grain-size distribution of the whole deposit, and the corresponding Mdϕ and $\sigma\phi$ parameters. The distribution was calculated based on 10 sample points, which include both the proximal and all the distal measured sections, with the most distal sample being at 25 km from the vent. At selected key sections, 26 samples of tephra were collected for grain-size analyses. Samples were dry-sieved at half-ϕ intervals ($\phi=-\log_2 D$, where D is the particle diameter in millimeters) for the coarser fraction. The fine-grained material (<0.25 mm) was sieved with water. Grain-size parameters were calculated following Inman (1952). The coarse fraction of 19 samples (≥1 mm, representing ≥40-50 wt.% in each sample) was analyzed for componentry, and components from each grain-size class were separated by hand picking under a binocular microscope and weighed. Two main categories were identified: juvenile material (which was further divided into vesicular fragments and obsidian), and lithics, including altered tuff, scoria and lavas. All the grain-size and componentry data are reported in Table 1. Morphology and texture of the different clast types were also described using thin sections and by imaging with scanning electron microscope (SEM). Density measurements, from a subset of six samples collected at the key sections (100 clasts each, for a total of 600 fragments), were performed on vesicular juvenile clasts in the grain size range $-3<\phi<-2$, following the method of Houghton and Wilson (1989). Clast densities were converted to vesicularity values using the DRE of 2,400 kg m^{-3}. Density and vesicularity distributions were also used to select clasts for quantitative textural (Vesicle Size Distribution) analysis following the method of Shea et al. (2010). Clasts were mounted in epoxy resin and prepared as polished thin sections. SEM back-scattered images were acquired at three different magnifications (50×, 150× and 300×) and processed using ImageJ software (imagej.nih.gov/ij/) and the *MatLab*®-based software FOAMS of Shea et al. (2010). Whole rock major and trace element chemical analyses were performed on vesicular, homogenous pumice clasts from eight samples; major and trace elements analyses were performed respectively by ICP-AES and ICP-MS after Lithium Borate fusion and acid digestion at ALS Seville (Spain) laboratories (see https://www.alsglobal.com/ for further details). Matrix glasses of the juvenile fraction were analyzed with a Zeiss EVO MA 10 SEM equipped with an Oxford Si(Li) energy-dispersive X-Ray detector (EDS) at Istituto Nazionale di Geofisica e Vulcanologia in Pisa (Italy). Analytical conditions for the SEM-EDS analyses were a 15 kV acceleration voltage and a probe current of ~300 pA, with a working distance of 8.5 mm, 100 s live time in raster mode, ZAF correction and natural minerals as calibration standards.

3. Results

3.1 Stratigraphy

The proximal deposits of the Baia – Fondi di Baia eruptive succession were mostly emplaced close to three nearly circular depressions which are today partly invaded by the sea at the harbour of Baia, about 15 km west of Naples (Fig. 1). The three depressions are aligned along a 2 km-long, N-S-trending structural alignment in the western part of the caldera. The northernmost depression, which is partly hidden by the sea, is the largest of the three having a radius of ~0.5 km and an area of 0.8 km^2. The central and southernmost of the circular depressions measure 0.12 and 0.20 km in radius, and occupy areas of 0.12 and 0.17 km^2, respectively. According to previous interpretations, these circular depressions represent three eruptive centres formed during the coeval eruption of Baia – Fondi di Baia (e.g. Rosi and Sbrana 1987). The tephra deposits overlie a paleosoil dated at 9525–9696 BP (Di Vito et al. 1999; Smith et al. 2011) and in proximal outcrops form a >20 m-thick succession of massive-to-stratified tephra beds and scattered ballistic bombs. This thick succession rapidly thins away from the rims of the three depressions, where most of the material was emplaced. Distal deposits, commonly represented by a single, cm-thick tephra layer, cover an area >60 km^2 and consist of white, aphyric, pumiceous lapilli with a few clasts of tuffs and lavas. The detailed study of stratigraphic relationships between the various tephra layers, their relative correlation among proximal outcrops and componentry of the deposits have allowed us to identify two eruptive sequences, represented by two respective successions of deposits. The lower succession, which has a maximum thickness along the cliffs in front of Baia's harbour (Fig. 1), is related to eruptive activity at a vent centred in the Baia depression. The uppermost succession crops out at the top of the southernmost depression and is related to an eruption from a vent located in the Fondi di Baia depression (Fig. 1). Both tephra successions lie above the same paleosoil, and in some cases the succession of Fondi di Baia lies directly above that of Baia, separated only by a reddish, mm-thick, reworked ash-bearing deposit.

3.2 The Baia succession

The key section of the Baia succession is exposed on the western side of Baia's harbour (33T 421794, 4519371; Section 1 in Fig. 1). Based on sedimentological features, the Baia succession can be divided into three main units (I to III), corresponding to three different stages of the eruption. At the outcrop scale, these features also allowed us to discriminate fallout from PDC deposits, which were also differentiate in dense, pyroclastic density current deposits and surge-like, turbulent current deposits.

Unit I: breccia deposit

The basal unit (Unit I) is a breccia deposit which lies on a dark-brown paleosoil (Fig. 2a). This breccia deposit is up to 3.5 m-thick and has a limited dispersal, with an abrupt decrease in thickness within a few hundred meters of the coastline. It includes cm-sized pumice and scoria clasts, m-sized blocks of yellow tuff, dark-reddish dense clasts and sparse beach pebbles embedded in a muddy, yellowish matrix. Both the matrix and the coarse material have evidence of pervasive alteration, with juvenile clasts (pumice) being partially or entirely substituted by yellowish-greenish to pinkish zeolite and clay minerals. The whole deposit is partially lithified, hampering sampling for detailed grain-size and componentry analyses.

Unit II: fallout-dominated deposits

The overlying unit (Unit II) consists of a 12 m-thick succession, with the lowermost 4 m consisting of coarse-grained, pumice-bearing parallel layers embedded in a fine-grained matrix. Matrix and juvenile clasts in some layers show strong alteration, similar to that of the underlying breccia, alternating with layers in which alteration is scarce-to-incipient (Fig. 2b, c). Dense, commonly banded, blocks and pumice bombs up to 50 cm in size (Fig. 2b, c) form impact sags in places. The upper part of Unit II has a progressive increase along the stratigraphic height in abundance and thickness of cross-bedded, ash-bearing deposits (Fig. 2d). Blocks and bombs, with diameters of up to 50 cm and often showing dense and breadcrusted rims, are common (Fig. 2e). The orientation of most impact sags suggests that the approximate position of the vent feeding Unit II did not coincide with the position of the hypothesized source of the opening breccia, but shifted in-land. All of the succession has a 9° dip to the south.

Most of the samples of Unit II have unimodal grain-size distributions, with a slight, coarse-tailed asymmetric shape, with Mdϕ ranging from -3.13ϕ to 2.54ϕ, and sorting values between 1.52 and 4.07ϕ (Fig. 3, Table 1). Among all the deposits of the Baia succession, Unit II corresponds to the peak in the grain-size.

Component analyses show that juvenile clasts account for >70 wt.% of the total deposit. The juvenile material is quite homogeneous and represented by vesicular, light-coloured pumice fragments, with pumice from the bottom of the tephra succession showing more pervasive alteration. Lithic clasts slightly decrease in abundance from the base of the sequence to the top and are represented by altered tuffs, red-oxidized clasts and minor lava fragments (Fig. 3).

Unit III: PDC-dominated deposits

Unit III, which stratigraphically represents the youngest part of the Baia succession, is a 6.5 m-thick succession of dm-thick, fine-to-coarse grained, laminated ash beds with dunes, antidunes and cross bedding structures (Fig. 2f). Most layers are lithic rich, including banded to dense juvenile clasts, and ash layers are thicker than in Unit II. A few bombs, which are smaller than those in the lower unit (maximum diameter: 10-20 cm), occur within Unit III and are mainly represented by juvenile dense bombs. No lithic blocks are observed. Depositional structures indicate a provenance of the PDCs being from the east. On top of Unit III, a soil separates the Baia succession from the deposits of the Averno 2 eruption as described by Di Vito et al. (2010), Fourmentraux et al. (2012) and Pistolesi et al. (2016).

Deposits of Unit III are finer than those of Unit II, with Mdϕ values ranging from -1.70ϕ to -1.14ϕ, and sorting values in the range 2.51ϕ-2.29ϕ (i.e. these are poorly to very poorly sorted deposits; Fig. 3, Table 1). Juvenile material, which accounts for 63 to 75 wt.% of the deposit, consists of vesicular pumice fragments and minor black, dense fragments. While most of the Unit III samples are enriched in the lithic component in the coarser grain-size classes (-4ϕ), the juvenile fraction usually dominates in the medium to finer grain-size classes (-3ϕ – 0ϕ). As a whole, the lithic fraction is higher with respect to Unit II (Fig. 3).

Distal deposits

The thick succession emplaced close to the source area rapidly thins out in a few hundred meters. Farther from the vent area, a tephra deposit has been identified up to 20 km north of the Baia crater. In medial to distal areas, this deposit consists of a single, massive layer of white to light brown pumice clasts. This layer is commonly sandwiched between two humic-rich soils, and its thickness ranges between 25 and 5 cm (Fig. 2g). Grain-size of mid-distal tephra samples have a large variability, with Mdϕ values ranging from -2.90ϕ (for more proximal samples) to 1.19ϕ (for distal samples along the dispersal axis), and $\sigma\phi$ values are typical of well-sorted to very poorly-sorted deposits (Table 1). Lithic clasts are scarce to absent, with most of the material represented by yellowish to light-brown, vesicular pumice clasts.

Based on the nature (colour and vesicularity) of the juvenile fraction, and on the sedimentological features (constant thickness at the outcrop scale and thinning from proximal to distal areas), this distal deposit has been correlated with the lower part of Unit II and it likely represents the main fallout phase. The maximum thickness of the fallout deposit in the proximal succession (i.e. sample BFB5 at section 1) is ~60 cm. In distal areas, the fallout layer is massive and lacks grading, whereas in the proximal area it is intercalated with PDC deposits and minor fallout beds.

3.3 The Fondi di Baia succession

The proximal deposits of the Fondi di Baia (FdB) succession crop out on the rim of the southern depression, close to the Castle of Baia (Fig. 1). At type section 2 (33T 421780, 4517497; Fig. 1), the succession overlies a tephra layer which in turn rests on a dark brown soil. This is interpreted as a fallout deposit from the Baia event (Unit II). A mm-thick, laterally continuous, oxidized ash layer separates Baia tephra from that of the FdB (Fig. 4a, b). The FdB deposits consist of two main units (IV and V).

Unit IV: breccia deposit

Unit IV is a one meter-thick, coarse breccia with limited dispersal, bearing yellowish to greenish meter-sized blocks of altered tuffs and pumice fragments. It bears juvenile bombs and differs from the basal breccia of the Baia succession (Unit I) by not containing a muddy altered matrix and beach pebbles.

Unit V: PDC-dominated deposits

Unit V overlies the breccia deposit and consists of 10-12-m thick, fine- to coarse-grained, stratified ash and pumice layers with intercalated ballistic obsidian bombs (Fig. 4c), which crop out at sections 2 and 3 (33T 422063, 4518067; Fig. 1). Mdϕ ranges between -2.53ϕ and 0.21ϕ, and the grain-size distribution has a positive skewness with a unimodal mesocurtic to platicurtic form. Sorting is usually poor, ranging from 3.02ϕ and 3.97ϕ (Fig. 3; Table 1).

Component analyses highlight that the juvenile fraction abundance in these Unit V samples is similar (50 to 90 wt.%) to that of the Baia succession, but contains up to 1.3 wt.% obsidian clasts. These clasts help to distinguish these FdB deposits from the Baia pyroclastic succession at the outcrop scale. Obsidian chips occur as fine-grained juvenile clasts, which possibly derive from impact-shattering of the skin of ballistic obsidian bombs.

3.4 Volume, column height and classification of the fallout phase

The volume obtained based on isopach maps (Fig. 5a) and calculated with different approaches is 0.06±0.008 km^3, which converts to a DRE volume of 0.02±0.002 km^3. The corresponding mass of the erupted material is $4.06\pm0.5 \times 10^{10}$ kg. This value is representative only of the fallout deposit. The volume of the material emplaced in proximal areas, and related to breccia and PDC deposits of both Baia and FdB successions, was estimated by integrating the dispersal of PDC deposits and their average thickness measured in the field yielding a total erupted mass of 0.01±0.004 km^3.

We also estimated the column height of the fallout phase of Unit II. The isopleth map (Fig. 5b) shows a slight eastward shift with respect to the isopach curves, possibly because maximum clast measurements record the peak of the fallout phase, but total thickness measurements might be related to multiple, juxtaposed fallout layers emplaced under variable wind conditions. From these isopleth maps we obtained an average column height of ~17 km, associated with a wind speed of 10-15 m s^{-1} at the tropopause and corresponding to a peak mass flow rate (MFR) of 1.8×10^7 kg s^{-1} or to a volumetric flow rate of 7.2×10^3 m^3 s^{-1}.

Given the complexity of classifying eruptions characterized by a large volume of tephra emplaced as PDC deposits, we consider here only the cumulative fallout phases for classification purposes. Based on erupted volume and mass, MFR, plume height, thickness, and grain-size data, the fallout phase of Unit II was classified. A total volume of 0.06±0.008 km^3 and a mass $4.06\pm0.5 \times 10^{10}$ kg result in a VEI 3 (Newhall and Self 1982) and a magnitude of 3.6, with the calculated MFR corresponding to an intensity of 10.2 (Pyle 2000). The plume developing during Unit II can be classified as subplinian based on the MFR versus plume height classification of Bonadonna and Costa (2013). Based on the thinning trend of the deposit, this phase can be also described by two exponential segments on a log(thickness) versus the square root of isopach area, with a corresponding bt value of 0.5 and 3.2 km, and therefore two values of bc/bt ratio (i.e., 3.6 and 0.6 from the isopleth map of Figure 5b). These parameters plot again in the field of subplinian eruptions following the classification scheme of Pyle (1989).

3.5 Total Grain-Size Distribution

The Total Grain-Size Distribution (TGSD) of a tephra deposit is an important eruptive parameter that has become more and more relevant in developing transport and sedimentation models, as well as in scenario definitions for volcanic hazard assessment (e.g., Costa et al. 2016). For our case, the TGSD has a polymodal grain-size distribution (Fig. 6) with $Md\phi$ = -1.9 and $\sigma\phi$ = -3.3, but with two modes at -3ϕ and 5ϕ. The almost complete lack of the 3ϕ grain-size class, along with the absence of a finer tail (>6ϕ), can be related to fragmentation processes coupled with the limited spatial distribution of the analyzed samples. Costa et al. (2016) explored the minimum sampling distances needed for a given size class normalized to column height (D/H, with D being the distance from the vent along the dispersal axis and H the plume height above vent, respectively). They found that a minimum sampling distance of ~60 km in low wind conditions was required to capture the distribution finer than 0ϕ. Due to the limited exposure and preservation of our distal sites, and based on the fact that our most distal sample is 25 km from the vent, we suggest that, following the plot presented in Costa et al. (2016), our reconstructed distribution underestimates the finer fraction of the TGSD.

3.6 General characteristics of the juvenile fraction

Juvenile clasts contain <5 vol.% phenocrysts. Mineral phases are usually euhedral and consist mainly of feldspars from 250 µm to 2 mm in size, with minor diopsidic clinopyroxene, biotite, spinel and apatite. Some dense clasts contain microlites, which are generally distributed randomly or are clustered in preferential zones. Most microlite dimensions are <100 µm. The observed mineralogy and its heterogeneity agree with the petrography previously described for trachytic-phonolitic products of CFc products (e.g. Rosi and Sbrana 1987; Armienti et al. 1983; D'Antonio e al. 1999; Smith et al. 2011).

Most of the fragments, irrespective of grain-size, display variable external and internal textures, grading from vesicular to dense clasts. One of the striking features of the juvenile fraction is layering, which occurs both in vesicular and dense juvenile clasts. In most fragments, layering corresponds to variations in vesicularity and microlite content and size; denser bands are microlite-rich and alternate with vesicular bands without microlites. Banding is particularly evident in juvenile bombs. In the Baia deposits, bombs are often characterized by breadcrust surfaces, with alternation of lighter and darker bands (Fig. 7a-d). In some cases (Unit II), dense, crystal-rich bombs are present. FdB deposits are, instead, characterized by the presence of bombs with obsidian skins. Among vesicular fragments, textures range from highly vesicular with collapsed vesicles to moderately vesicular, with tabular aspects, to microvesicular. Vesicles show heterogeneous size and shapes and are often coalescent or tubular (Fig. 7e). Dense fragments are characterized by smaller vesicles and have a glassy groundmass (Fig. 7f). In dense, obsidian clasts, vesicles are often completely lacking.

3.7 Clast density and vesicularity

Density analyses were carried out on six samples, five belonging to the Baia succession and one to the FdB deposits. Three samples were selected from the main fallout phase (Unit II): BFB5 was sampled at section 1, whereas samples BFB1 and BFB17 were from medial areas along the border of the central depression and 0.4 km from section 1. Samples BFB7 and

BFB9 were from pyroclastic flow and surge deposits of Units II and III, respectively, as collected at section 1. Finally, sample BFB37 is representative of the pyroclastic flow deposit of Unit V from the FdB succession (section 3). Density analyses were performed on the $-3<\phi<-2$ size range and did not include the high density obsidian bombs identified at the outcrop scale. The analysis thus does not cover the full spectrum of clast density.

Samples from the fallout phase of Unit II (BFB1, 5 and 17) are characterized by slightly asymmetrical unimodal distributions, with a density range between 200 and 1900 kg/m^3 and a modal value of 500 kg m^{-3}. BFB7 has a bimodal density distribution, with a range between 200 and 1900 kg m^{-3} and with modes at 300 and 500 kg m^{-3} (average density of 740 kg m^{-3}). BFB9 has a polymodal trend with a density range between 400 and 1300 kg m^{-3}, and modes at 500, 700 and 1000 kg m^{-3}, and an average density of 740 kg m^{-3}. Finally, BFB37 has a unimodal, asymmetric distribution, with a range of densities between 600 and 1300 kg m^{-3} and a mode at 910 kg m^{-3} (Fig. 8). In general, while the fallout phase is characterized by lower density clasts and narrower variations, density values tend to increase towards the top of the succession, also showing progressively larger variations. Using a clast density of 2400 kg m^{-3}, density values were converted to vesicularity values that ranged between 62 and 79 vol.% (Figs. 8, 9, Table 2).

3.8 Textural analyses

Textural data were collected on the same sample set as used for density analyses, except for the fallout phase of Unit II for which only one sample (BFB5, section 1) was analyzed. From the density distributions, clasts representative of the modal (MD), low-density (LD) and high-density (HD) end-members were chosen for each sample (Fig. S1 in the Supplementary Material). Vesicles show a wide range of variability, including heterogeneous size and shape. Vesicles vary from circular to elongated, up to tubular.

The results of the textural analysis are summarized in Table 3. In general, vesicle sizes display a quite narrow range (0.01-2.10 mm) with maximum values observed in LD samples. In contrast, HD samples always have the lowest values of maximum size, with MD samples displaying intermediate values. Vesicle Volume Distributions (VVDs; Fig. 10) are unimodal to bimodal. MD clasts are generally characterized by symmetric Gaussian distributions with a mode ranging between 0.08 and 0.14 mm, and the lowest value recorded in the fallout phase of Unit II (BFB5) which was 0.005 mm. LD clasts have a similar distribution at low vesicle sizes (modal L = 0.14-0.18 mm) but display a secondary mode of larger vesicles (L > 1 mm). HD samples are also characterized by a similar distribution of small vesicles (modal L = 0.14 mm), but in this case the distribution appears truncated at large vesicle sizes.

Total Vesicle Number Densities (VNDs) are in the range of $2 \times 10^7 – 1 \times 10^8$ cm^{-3} and were extracted from the Cumulative Vesicle Size Distribution (Fig. S2 in the Supplementary Material) as listed in Table S1. For each stratigraphic level, the highest VNDs were found in an MD sample. The only exception was BFB7 (Unit II – flow phase) for which the HD sample have a relatively higher value. With increasing stratigraphic height during the Baia eruption (Fig. 9), VNDs of modal density clasts decrease from a maximum value of 1×10^8 cm^{-3} in sample BFB5 (Unit II – fallout phase) to 4.5×10^7 and 4.2×10^7 cm^{-3} for sample BFB7 (Unit II - flow phase) and sample BFB9 (Unit III - surge phase). The unique sample (BFB37) related to the FdB deposits (Unit V) is instead characterized by a higher VND value (8.1×10^7 cm^{-3}) closer to the VND of the initial phase of the Baia event. VND values of HD samples are generally comparable with those of LD samples, except for BFB7 (Unit II – flow), which was a value three times greater than the corresponding LD sample.

Following the strategy of Shea et al. (2011), we used the textural parameters (i.e. VND) to estimate the maximum decompression rate (dP/dt) at fragmentation using the method of Toramaru et al. (2006). The calculations were performed on all the analyzed samples and the results are listed in Table S1. To capture the decompression rates corresponding to the final stage of rapid ascent prior to fragmentation, VNDs were recalculated (VND_{corr} in Tab. 3) for the vesicle range of 0.01-0.001 mm (Shea et al. 2011). Calculations were completed using: (i) T = 945 °C (Piochi et al. 2008); (ii) P = 100 MPa (corresponding to a depth of ~4 km); (iii) H_2O = 1.5 wt% (the amount of water at saturation conditions at that depth following Arienzo et al. 2010); (iv) melt density of 2400 kg m^{-3} (calculated on chemical basis at T and P with the model by Lange and Carmichael (1987)); (v) water diffusivity of 2.35×10^{-11} m^2 s^{-1} (Freda et al. 2003); and (vi) surface tension of 0.035 N m^{-1} (Shea et al. 2011). Calculated decompression rates range between 0.20 and 0.69 MPa s^{-1} (or 0.37 - 0.69 MPa s^{-1}, if only MD clasts are considered). Their variation follows the same trend of total VNDs (Fig. 9). While the highest values (0.68-0.69 MPa s^{-1}) are found for the MD clasts of the fallout samples (BFB5 – Unit II; BFB37 – Unit V), PDC-dominated (BFB7 – Unit II) and surge-dominated (BFB9 – Unit III) samples are characterized by lower decompression rates (0.34 - 0.36 MPa s^{-1} for MD clasts).

3.9 Chemistry

The compositions of products emitted during the Baia – Fondi di Baia eruption were classified by Rosi and Sbrana (1987) as being fairly homogenous alkali-trachyte. On the other hand, Smith et al. (2011) found variable glass compositions, ranging from 61.08 to 63.84 wt.% SiO_2 and 1.58 to 4.25 wt.% FeO, and also pointed to highly variable Cl contents (~0.65 to ~1.15 wt.%). Whole rock compositions representative of the two eruptive successions presented in this paper span a narrow range in the trachyte field, with SiO_2 of 62.1 - 64.9 wt.% and Na_2O+ K_2O of 10.5 - 13.5 wt.%. FdB samples have slightly higher alkali contents (Fig. 11). It is worth noting that some of the analyzed samples have high LOI (Loss On Ignition) values. Due to this, and based on the fact that the juvenile fraction shows a large textural variability, we decided to check the whole rock data with a groundmass glass investigation. Vesicular and dense fragments were selected and mounted for the Baia succession (250 clasts) from Units II and III and from the FdB deposits (160 clasts) from Unit V. Analyses, normalized to anhydrous composition, reveal that glass products span a wide range of compositions from tephriphonolites at the boundary with latites (SiO_2 of 56.6 wt.% alkali content of 10.4 wt.%) up to phonolites (SiO_2 61.4 wt.%, alkali 13.60 wt.%) to trachytes (SiO_2 between 62 and 64 wt.%, alkali between 13.4 and 10.32 wt.%). These ranges are even larger than those presented in Smith et al. (2011), with the FdB products having the largest variability (Figs. 9, 10). No correlation is evident between clast texture and composition where, for both eruptive successions, glass analyses of vesicular and dense clasts show both tephriphonolitic compositions and more differentiated phonolitic-trachytic compositions.

The Baia products comprise mainly trachytic compositions, with the least evolved tephriphonolitic magma appearing only during the first part of the main eruptive phase (Unit II) and only among finer-grained juvenile clasts. The tephriphonolitic-phonolitic compositions apparently lack in the final stages of the Baia eruptive succession (Unit III). However, during Unit V of the FdB episode, all compositions were contemporaneously tapped, with a sharp increase in the proportion of tephriphonolitic and trachytic compositions, as discussed in detail in Voloschina (2016). While trachytic compositions correlate well with most of the Campi Flegrei eruptive products, tephriphonolitic compositions are generally poorly represented within Campi Flegrei magmas (c.f., Orsi et al. 1995; D'Antonio et al. 1999; De Vita et al. 1999; Tonarini et al. 2009; Di Renzo et al. 2011).

4. Discussion

4.1 Dynamics of the Baia and Fondi di Baia eruption

Coupling the reconstructed architecture of the tephra deposits with sedimentological and textural data, we interpreted the tephra successions and different units to reconstruct the sequence of eruptive events that built the Baia – Fondi di Baia sequence. We suggest that the Baia and the FdB deposits belong to the same eruption, but are the result of two different eruptive episodes separated by a short time break (Fig. 12). The Baia phase began in an area close to the present coastline. Based on deposit dispersal and the morphology of the area, the inferred vent can be located in the centre of Baia's harbour. The opening phase of the eruption (Unit I) excavated the shallow basement material consisting of tuffs, which are the main component of the lithic material within the coarse-grained, low-dispersed breccia deposits. This was the opening stage of the Baia episode. Strong alteration, presence of muddy matrix and beach pebbles also confirm that the opening phase occurred in a shallow-water environment. The dispersal and orientation of the breccia deposit suggest that it was only partially emplaced on-land, on a dark brown paleosoil, where it formed the landward side of a growing littoral cone, with most of the material being emplaced in, and rapidly dispersed by, the sea.

The eruption rapidly escalated to its climax (Unit II), during which fallout layers and pyroclastic density current deposits were emplaced. While the lower part of Unit II is dominated by fallout activity, with a fall/PDC ratio of >1, the upper part shows a progressive decrease in the ratio, as highlighted by the increase of ash-bearing and internal stratification of tephra layers. The eruptive column responsible for the fallout activity at the beginning of Unit II had a maximum height of 17 km and dispersed tephra northward to form a deposit with a volume of 0.06±0.008 km^3. The TGSD of the related fallout deposit was polymodal, as observed for other plinian-subplinian deposits (e.g. Mount St Helens 1980, Cordón Caulle 2011 – Unit I, Askja 1875 phases C and D; Durant et al. 2009, Bonadonna et al. 2015, Sparks et al. 1981), with the 3ϕ size class being almost absent. The gradual disappearance in Unit II of the muddy, altered matrix associated with the presence of ballistic bomb sags suggests that the eruptive vent during this phase progressively migrated on-land. The intensity of the eruption began to decline during the final phase of Unit II, when PDCs formed deposits embedded with many ballistic blocks, possibly related to increasingly unsteady eruptive conditions that did not favour development of a sustained column. The abundance of large ballistic blocks embedded in the PDC deposits indicates that activity was accompanied by violent explosions, supporting a model whereby the phase of the eruption was characterized by a pulsating behaviour.

The dynamics of the final phase of the Baia sequence shifted toward more turbulent, surge-like, PDC activity, during which dune-bedded deposits were emplaced (Unit III). No clear fallout layers were distinguished within this unit. Textural and sedimentological data suggest that this final phase resulted from a lower magma ascent rate during an intermittent, Vulcanian-like activity, as suggested by the increase both in density of juvenile clasts and lithic content of the deposits.

The general decrease of the eruption intensity during the Baia episode is consistent with a peak of intensity during the initial part of Unit II, during which the highest vesicularity (81 vol.%), the highest VNDs (1×10^8 cm^{-3}) and the highest decompression rate (0.69 MPa s^{-1}) were recorded. All of these parameters progressively decreased through Units II and III, possibly due to a reduction of magma ascent rate with time. The main process controlling the evolution of the eruption dynamics was a progressive degassing of the magma, with more evident gas-melt decoupling during the final phases of the eruption. The absence of important microlite growth from Unit I to Unit III suggests, however, that the eruption was probably short and that degassing did not induce undercooling.

Within the same stratigraphic level, the presence of clasts of various density appears to be related to variable degrees of vesicle evolution by coalescence (LD samples) or removal of larger sizes (HD). All classes appear to be genetically related, with the modal samples representing magma degassing under closed conditions at the local scale (Gaussian VVD distribution) and relatively fast ascent rates (small modal vesicle sizes and high VNDs). For LD samples, the presence of a secondary mode at large vesicle sizes, coupled with lower VNDs, indicate that these clasts sampled part of an ascending magma characterized by higher degrees of bubble growth due to coalescence, as testified by the presence of retracted melt films along the rims of larger vesicles (see Fig. S1 in the Supplementary Material). Conversely, for HD clasts, the absence of large vesicles can be related to efficient gas percolation through pathways in the magma (e.g., outgassing) and compaction, as testified by collapsed structures (Fig. S1 in the Supplementary Material). This process most likely takes place at the conduit wall, where magma ascent velocity is lower (D'Oriano et al. 2011).

After the end of the Baia episode, a short stasis in the activity followed. This was marked by the presence of a mm-thick, oxidized ash layer (Fig. 4a) which directly overlies the Unit II fallout deposits in the southern sector, where no PDC deposits related to the Baia tephra succession were found. The lateral continuity of the reddish ash layer can be related to oxidation and/or humification which likely marks a short stasis in the eruptive sequence. Activity re-commenced with the opening phase of the FdB eruptive episode (Unit IV) from the southernmost crater. The central depression was unlikely the FdB eruptive centre because its floor is covered by the soil over which Units II and III are emplaced and which form the crater walls. The depression possibly pre-dated the eruption, or was formed by post-eruption collapse along the same N-S structure along which the vents are aligned.

The FdB opening phase involved the same substratum of tuff, which was mixed with the breccia, but did not occur in a shallow-water environment. In fact, the FdB opening breccia deposit (Unit IV) consists of altered tuff blocks and greenish ash, but lacks beach pebbles and the pervasive alteration of the juvenile fraction observed in Unit I of the Baia deposits. After the opening breccia-emplacing phase, the eruption evolved towards PDC activity (Unit V), which strongly resembled that of the final part of Unit II. No fallout deposits can be clearly identified within Unit V. The striking feature of the FdB eruptive units is a lower dispersal compared with those of the Baia eruption, a lack of clear fallout layers, and the presence of obsidian clasts. Textural data on juvenile clasts also reveal higher clast densities and lower VNDs with respect to the peak phase of Baia, suggesting that eruption intensity was lower than in the initial Baia event with a partial recovery in the eruption intensity during the FdB episode. Calculated decompression rates for Unit V (0.68 MPa s^{-1}) are, however, comparable with those inferred for the initial phase of the Baia sequence. This is possibly due to higher volatile contents, coupled with higher groundmass crystallinity or higher nucleation due to higher volatiles oversaturation during the Baia episode. It should be noted that decompression rate calculations were performed under the assumption of water saturation at depth. However, if these conditions are not met, calculated decompression rates can dramatically decrease. Moreover, the elevated density of juvenile clasts (and the presence of obsidian clasts) would suggest a degassing process under open conditions, where outgassing can deeply modify the juvenile textures used for decompression rate calculations.

The direction along which vents migrated during the eruptions coincides with a N-S trend which follows a structural boundary (Vitale and Isaia 2014) and this boundary apparently controls the eruptive activity in the western part of the caldera. Most of the vents in this area (Mofete, Bellavista, Bacoli, Porto Miseno, Averno 1 and Averno 2, Baia and Fondi di Baia) are in fact aligned along this main trend (Bevilacqua et al. 2015).

4.2 Variability of magma composition

Bulk rock analyses show a narrow trachytic compositional range among the products of the two eruptive events. However, a more detailed investigation of the groundmass glass compositions carried out both on single, mm-sized clasts and dm-sized bombs revealed a larger variability from tephriphonolites-latites, to phonolites, to trachytes. Baia's eruptive products display a wider variability within trachytic compositions. On the other hand, FdB groundmass compositions cover a wider field than less evolved tephriphonolitic compositions. The absence of correlation between clast texture and composition, with vesicular and dense clasts characterized by both weakly evolved and more differentiated compositions, suggest that the textural variability is related to ascent rate or magma/conduit interactions. The chemical variability, however, suggests that the eruptive episodes were fed by a complex reservoir, or different reservoirs, which was (or were) progressively drained during the course of the two events, with an increasing involvement of less evolved magma during the FdB phase. Moreover, because larger clasts and bombs were commonly associated with trachytic compositions, we speculate that most of the magma volume during the eruption was a trachyte.

4.3 Magmatic versus phreatomagmatic fragmentation

Distinctive surface textures (stepped surfaces, quench cracks, and pitting) or morphology (e.g. blocky clasts) of juvenile material have been traditionally interpreted as being derived from magma-water interaction (Heiken and Wohletz 1985; Kokelaar 1986; Büttner et al. 1999; Cioni et al. 2014). Variations in the morphological features of the clasts can, however, be interpreted in terms of the relative role played by different fragmentation processes during an eruption. Interaction with external water during the Baia phase is indicated by the presence of an altered, muddy matrix and rounded beach pebbles in the opening breccia. The migration of the vent progressively hampered the access of seawater to the erupting magma, although a certain degree of interaction cannot be ruled out during the early phase of Unit II, which also corresponds to the peak phase of the eruption. Textural data indicate that fragmentation occurred over a heterogeneous magma column characterized by variable vesicularity. The ubiquitous predominance of highly vesicular fragments at all stratigraphic levels and the lack of clear magma-water interaction textures indicate a prominent active role of degassing-related magmatic fragmentation during the eruption. The interaction with seawater would have occurred at the crater level with an already fragmented magma, strongly influencing the external dynamics (tephra dispersal and sedimentation) of the eruption and the following, post-emplacement alteration, without making an important contribution to the fragmentation process. The obsidian clasts within the FdB deposits, on the other hand, may be unrelated to magma-water interaction because the vent already had migrated on-land, although possible seawater or groundwater infiltration cannot be completely excluded. The occurrence of clasts of obsidian, which also forms skins on bombs, can be more likely attributed to magma/conduit interaction and/or slower magma ascent rates.

5. Conclusions

After a 1000 year-long period of quiescence, eruptive activity at Campi Flegrei renewed at 9525–9696 BP with one of the sporadic eruptions that characterize those of the western sector of the caldera. Understanding the dynamics of this complex event is particularly relevant, as it opens Epoch 2 of activity at CFc, marking the passage from a period of quiescence to a new cycle of intense volcanic activity. Although small in terms of volume with respect to most of the post-NYT events, the Baia – Fondi di Baia eruption was characterized by complex dynamics and deposit features similar to other volcanoes of the CFc western sector. Based on a detailed stratigraphic study, and sedimentological and textural analyses of the tephra deposits, we divided the eruptive event into two, time-separated sequences, which share some common characteristics. The Baia eruptive episode began in a shallow-water environment with the emplacement of a breccia (Unit I), rapidly followed by an alternation of fallout and PDC emplacement deposits (Unit II). Sedimentological and textural analyses suggest that this was the peak phase of the eruption, which progressively waned to surge activity associated with Vulcanian-like explosions (Unit III). The passage from Unit I to Units II-III was also marked by a vent shift, which moved on-land. The nature of the deposits also suggests that, during this phase, the fragmentation was purely magmatic. After a short pause, the eruptive activity renewed with the onset of the Fondi di Baia episode, south of the Baia crater and along a N-S structural alignment, which represents a structural boundary of the caldera. The new activity was represented by a second breccia deposit (Unit IV), which marked the onset of the FdB event. The final phase of the eruption (Unit V) partly resembles that during the final stage of Unit II, apart from the presence of obsidian clasts and the lack of clear fallout layers. Textural features of the juvenile fraction (lower vesicularity and VNDs) also indicate lower intensity during this phase. The large range of groundmass glass compositions, related to differing proportions among more (phonolitic-trachytic) and less (tephriphonolitic-latitic) evolved end-members, also suggests that the eruption was fed by a complex reservoir. This was progressively drained during the course of the two eruptive sequences, with an increase of less evolved magma during the Fondi di Baia episode, but with the majority of the magma volume involved being represented by the more evolved composition.

Acknowledgments

This study was funded by the "Project V1: Probabilistic Volcanic Hazard Analysis" in the framework of the agreement between Dipartimento di Protezione Civile e Istituto Nazionale di Geofisica e Vulcanologia (Reasearch Unit UNIFI, responsible M. Pistolesi). We thank F. Mazzone and M. Voloschina for lab analyses, M. Pompilio, M. Rosi, C. Romano and S. Campagnola for discussions in the field. D. Mazzarella is greatly thanked for having provided access to his private properties. We are also grateful to D. Swanson and to an anonymous reviewer for their constructive comments and to C. Bonadonna for editorial handling.

References

Armienti P, Barberi F, Bizouard H, Clocchiatti R, Innocenti F, Metrich N, Rosi M, Sbrana A (1983) The Phlegraean Fields: magma evolution within a shallow chamber. J Volcanol Geotherm Res 17:289 – 311.

Arienzo I, Moretti R, Civetta L, Orsi G, Papale P (2010) The feeding system of Agnano-Monte Spina eruption (Campi Flegrei, Italy): dragging the past into the present activity and future scenarios. Chem Geol 270 (1-4):135 – 147.

Barberi F, Corrado G, Innocenti F, Luongo G (1984) Phlegrean Fields 1982-1984: brief chronicle of a volcano emergency in a densely populated area. Bull Volcanol 47(2):175 – 185.

Barberi F, Carapezza M, Innocenti F, Luongo G, Santacroce R (1989) The problem of volcanic unrest: the Phlegrean Fields case history. Atti Conv Lincei 80:387 – 405.

Bevilacqua A, Isaia R, Neri A, Vitale S, Aspinall WP, Bisson M, Flandoli F, Baxter PJ, Bertagnini A, Esposti Ongaro T, Iannuzzi E, Pistolesi M, Rosi M (2015) Quantifying volcanic hazard at Campi Flegrei caldera (Italy) with uncertainty assessment: 1. Vent opening maps. J Geophys Res Solid Earth 120:2309–2329.

Bonadonna C, Houghton BF (2005) Total grainsize distribution and volume of tephra-fall deposits. Bull Volcanol 67:441–456.

Bonadonna C, Cioni R, Pistolesi M, Connor CB, Scollo S, Pioli M, Rosi M (2013) Determination of the largest clast sizes of tephra deposits for the characterization of explosive eruptions: A study of the IAVCEI commission on tephra hazard modelling, Bull Volcanol 75(1):1–15, doi:10.1007/s00445-012-0680-3.

Bonadonna C, and Costa A (2013) Plume height, volume, and classification of explosive volcanic eruptions based on the Weibull function. Bull Volcanol 75(8):1–19, doi:10.1007/s00445-013-0742-1.

Bonadonna C, Cioni R, Pistolesi M, Elissondo M, Baumann V (2015) Sedimentation of long-lasting wind-affected volcanic plumes: the example of the 2011 rhyolitic Cordón Caulle eruption, Chile. Bull Volcanol 77(13):1–19, doi:10.1007/s00445-015-0900-8.

Büttner R, Dellino P, Zimanowski B (1999) Identifying magma–water interaction from the surface features of ash particles. Nature 401:688–690.

Carey SN, Sparks RSJ (1986) Quantitative models of the fallout and dispersal of tephra from volcanic eruption columns. Bull Volcanol 48:109–125.

Chiodini G, Caliro S, De Martino P, Avino R, Gherardi F (2012) Early signals of new volcanic unrest at Campi Flegrei caldera? Insights from geochemical data and physical simulations. Geology 40:943 – 946.

Chiodini G, Vandemeulebrouck J, Caliro S, D'Auria L, De Martino P, Mangiacapra A, Petrillo Z (2015) Evidence of thermal-driven processes triggering the 2005-2014 unrest at Campi Flegrei caldera. Earth Planet Sci Lett 414:58 – 67.

Chiodini G, Paonita A, Aiuppa A, Costa A, Caliro S, De Martino P, Acocella V and Vandemeulebrouck J (2016). Magmas near the critical degassing pressure drive volcanic unrest towards a critical state. Nature Comm, 7:13712, DOI:10.1038/ncomms13712.

Cioni R, Pistolesi M, Bertagnini A, Bonadonna C, Hoskuldsson A, Scateni B (2014) Insights into the dynamics and evolution of the 2010 Eyjafjallajökull summit eruption (Iceland) provided by volcanic ash textures. Earth Planet Sci Lett 394:111–123, doi: 10.1016/j.epsl.2014.02.051.

Civetta L, Orsi G, Pappalardo L, Fisher RV, Heiken G, Ort M (1997) Geochemical zoning, mingling, eruptive dynamics and depositional processes – the Campanian Ignimbrite, Campi Flegrei Caldera, Italy. J Volcanol Geotherm Res 75:183 – 219.

Costa A, Pioli L, Bonadonna C (2016) Assessing tephra total grain-size distribution: Insights from field data analysis. Earth Planet Sci Lett 443:90–107.

Crandell DR (1989) Gigantic debris avalanche of Pleistocene age from ancestral Mount Shasta volcano, California and debris-avalanche hazard zonation. USGS Bull, 1861.

D'Antonio M, Civetta L, Orsi G, Pappalardo L, Piochi M, Carandente A, De Vita S, Di Vito MA, Isaia R, Southon J (1999) The present state of the magmatic system of the Campi Flegrei caldera based on the reconstruction of its behaviour in the past 12 ka. J Volcanol Geotherm Res 91:247 – 268.

D'Oriano C, Poggianti E, Bertagnini A, Cioni R, Landi P, Polacci M, Rosi M (2005) Changes in eruptive style during the A.D. 1538 Monte Nuovo eruption (Phlegrean Fields, Italy): the role of syn-eruptive crystallization. Bull Volcanol 67:601 – 621.

D'Oriano C, Cioni R, Bertagnini A, Andronico D, and Cole PD (2011) Dynamics of ash-dominated eruptions at Vesuvius: the post-512 AD AS1a event. Bull Volcanol 73(6):699–715, doi: 10.1007/s00445-010-0432-1.

Deino AL, Orsi G, De Vita S, Piochi M (2004) The age of the Neapolitan Yellow Tuff caldera-forming eruption (Campi Flegrei caldera – Italy) assessed by 40Ar/39Ar dating method. J Volcanol Geotherm Res 133:157 – 170.

De Vita S, Orsi G, Civetta L, Carandente A, D'Antonio M, Di Cesare T, Di Vito M, Fisher RV, Isaia R, Marotta E, Ort M, Pappalardo L, Piochi M, Southon J (1999) The Agnano-Monte Spina eruption (4.1 ka) in the resurgent, nested Campi Flegrei caldera (Italy). J Volcanol Geotherm Res 91:269 – 301.

Di Renzo V, Arienzo I, Civetta L, D´Antonio M, Tonarini S, Di Vito MA, Orsi G (2011) The magmatic feeding system of the Campi Flegrei caldera: architecture and temporal evolution. Chem Geol 281:227 – 241.

Di Vito MA, Isaia R, Orsi G, Southon J, de Vita S, D'Antonio M, Pappalardo L, Piochi M (1999) Volcanism and deformation since 12,000 years at the Campi Flegrei caldera (Italy). J Volcanol and Geotherm Res 91:221 – 246.

Di Vito MA, Arienzo I, Briar G, Civetta L, D'Antonio M, Di Renzo V, Orsi G (2010) The Averno 2 fissure eruption: a recent small-size explosive event at the Campi Flegrei Caldera (Italy). Bull Volcanol 73:295 – 320.

Durant AJ, Rose WI, Sarna-Wojcicki AM, Carey S, Volentik ACM (2009) Hydrometeor-enhanced tephra sedimentation: constraints from the 18 May 1980 eruption of Mount St. Helens. J Geophys Res 114 (B3):B03204. http:// dx.doi.org/10.1029/2008JB005756.

Fierstein J, Nathenson M (1992) Another look at the calculation of tephra volumes. Bull Volcanol 54:156–167

Fourmentraux, C, Métrich N, Bertagnini A, Rosi M (2012) Crystal fractionation, magma step ascent, and syn-eruptive mingling: the Averno 2 eruption (Phlegraean Fields, Italy). Contrib Mineral Petrol 163:1121 – 1137.

Freda C, Baker DR, Romano C, Scarlato P (2003) Water diffusion in natural potassic melts. Geol Soc London Spec Publ 213:53–62.

Giaccio B, Hajdas I, Isaia R, Deino A, Nomade S (2017) High-precision 14C and 40Ar/39 Ar dating of the Campanian Ignimbrite (Y-5) reconciles the time-scales of climatic-cultural processes at 40 ka. Sci Rep 7, 2017, 45940

Guidoboni E, Ciuccarelli C (2011) The Campi Flegrei caldera: historical revision and new data on seismic crises, bradyseisms, the Monte Nuovo eruption and ensuing earthquakes (twelfth century 1582 AD). Bull Volcanol (2011) 73: 655. doi:10.1007/s00445-010-0430-3

Heiken G, Wohletz KH (1985) Volcanic Ash. University of California Press, Berkeley. 245 pp.

Houghton BF, Wilson CJN (1989) A vesicularity index for pyroclastic deposits. Bull Volcanol 51:451–462

Inman DL (1952) Measures for describing the size distribution of sediments. J Sed Pet 22:125–145.

Isaia R, Marianelli P, Sbrana A (2009) Caldera unrest prior to intense volcanism in Campi Flegrei (Italy) at 4.0 ka B.P.: implications for caldera dynamics and future eruptive scenarios. Geoph Res Lett 36:L21303.

Kokelaar P (1986) Magma–water interactions in subaqueous and emergent basaltic. Bull Volcanol 48:275–289.

Lange RA, Carmichael ISE (1987) Densities of Na2O-K2O-MgO-MgO-FeO-Fe2O3-A l3O3-TiO2-SiO2 liquids: New measurements and derived partial molar properties. Geochim Cosmochim Acta 51:2931–2946, doi: 10.1016/0016-7037(87)90368-1

Le Maitre RW (1989) In: Bateman P, Dudek A, Keller J, Lameyr J, Le Bas MJ, Sabine PJ, Schmid R, Sørensen H, Streckeisen A, Woolley AR, Zanettin B (Eds.) A Classification of Igneous Rocks and Glossary of Terms: Recommendations of the International Union of Geological Sciences Subcommission on the Systematics of Igneous Rocks. Blackwell Scientific Publications, Trowbridge, Wilts, England, pp. 1 – 193.

Mastin LG, Guffanti M, Servranckx R, Webley P, Barsotti S, Dean K, Durant A, Ewert JW, Neri A, Rose WI, Schneider D, Siebert L, Stunder B, Swanson G, Tupper A., Volentik A., Waythomas C.F. (2009) A multidisciplinary effort to assign realistic source parameters to models of volcanic ash-cloud transport and dispersion during eruptions: J Volcanol Geotherm Res 186(1-2):10–21, doi:10.1016/j.jvolgeores.2009.01.008.

Newhall CG, and Self S (1982) The volcanic explosivity index (VEI): An estimate of explosive magnitude for historical volcanism, J Geophys Res 87(NC2):1231–1238, doi:10.1029/JC087iC02p01231.

Orsi G, D´Antonio M, De Vita S, Gallo G (1992) The Neapolitan Yellow Tuff, a large-magnitude trachytic phreatoplinian eruption: eruptive dynamics, magma withdrawal and caldera collapse. J Volcanol Geotherm Res 53:275 – 287.

Orsi G, Civetta L, D´Antonio M, Di Girolamo P, Piochi M (1995) Step-filling and development of three layer magma chamber: the Neapolitan Yellow Tuff case history. J Volcanol Geotherm Res 67:291 – 312.

Orsi G, Di Vito MA, Isaia R (2004) Volcanic hazard assessment at the restless Campi Flegrei caldera. Bull Volcanol 66:514 – 530.

Piochi M, Polacci M, De Astis G, et al. (2008) Texture and composition of pumices and scoriae from the Campi Flegrei caldera (Italy): Implications on the dynamics of explosive eruptions. Geochemistry Geophys Geosystems 9:Q03013. doi: 10.1029/2007GC001746

Pistolesi, M., Isaia, R., Marianelli, P., Bertagnini, A., Fourmentraux, C., Albert, P.G., Tomlinson, E.L., Menzies, M.A., Rosi, M., and Sbrana, A. (2016) Simultaneous eruptions from multiple vents at Campi Flegrei (Italy) highlight new eruption processes at calderas. Geology 44(6):487–490, doi: 10.1130/G37870.1.

Pyle DM (1989) The thickness, volume and grain size of tephra fall deposits, Bull Volcanol 51(1):1–15.

Pyle DM (2000) Sizes of volcanic eruptions, in Encyclopedia of Volcanoes, ed. H. Sigurdsson et al, 263–269, Academic Press, San Diego, California.

Rosi M, Sbrana A (eds) (1987) The Phlegraean Fields. Quad Ric Sci CNR Rome, 114, 10:175 pp.

Scarpati C, Cole P, Perrotta A (1993) The Neapolitan Yellow Tuff—A large volume mutiphase eruption from Campi Flegrei, Southern Italy. Bull Volcanol 55:343–356

Shea T, Houghton BF, Gurioli L, Cashman KV, Hammer JE, Hobden BJ (2010) Textural studies of vesicles in volcanic rocks: An integrated methodology. J Volcanol Geotherm Res 190:271–289. doi: 10.1016/j.jvolgeores.2009.12.003

Shea T, Gurioli L, Houghton BF, Cioni R, Cashman KV (2011) Column collapse and generation of pyroclastic density currents during the A.D. 79 eruption of Vesuvius: The role of pyroclast density. Geology 39:695–698, doi: 10.1130/G32092.1

Smith VC, Isaia R, Pearce NJG (2011) Tephrostratigraphy and glass compositions of post-15 kyr Campi Flegrei eruptions: implications for eruption history and chronostratigraphic markers. Quat Sci Rev 30:3638 – 3660.

Smith, V.C., Isaia, R., Engwell, S.L. Albert, P.G. Bull Volcanol (2016) 78: 45. doi:10.1007/s00445-016-1037-0

Sparks RSJ, Wilson L, Sigurdsson H (1981) The pyroclastic deposits of the 1875 eruption of Askja, Iceland. Philos Trans R Soc Lond 229:241–273.

Tarquini S, Isola I, Favalli M, Mazzarini F, Bisson M, Pareschi MT, Boschi E (2007) TINITALY/01: a new Triangular Irregular Network of Italy. Ann Geoph 50(3):407 – 425.

Tonarini S, D´Antonio M, Di Vito MA, Orsi G, Carandente A (2009) Geochemical and B-Sr-Nd isotopic evidence for mingling and mixing processes in the magmatic system feeding the Astroni volcano (4.1-3.8 ka) within the Campi Flegrei caldera (South Italy). Lithos 107:135 – 151.

Toramaru A (2006) BND (bubble number density) decompression rate meter for explosive volcanic eruptions. J Volcanol Geotherm Res 154:303–316. doi: 10.1016/j.jvolgeores.2006.03.027

Vilardo G, Isaia R, Ventura G, De Martino P, Terranova C (2010) InSAR permanent scatterer analysis reveals fault reactivation during inflation and deflation episodes at Campi Flegrei caldera. Remote Sens Environ 114:2373 – 2383.

Vitale S, Isaia R. (2014) Fractures and faults in volcanic rocks (Campi Flegrei, Southern Italy): Insights into volcano-tectonic processes. Int J Earth Sci 103:801–819. doi:10.1007/s00531-013-0979-0.

Voloschina M (2016) Compositional studies of the Baia – Fondi di Baia eruption, Campi Flegrei, Italy: insights into the magmatic system. Dipartimento di Scienze della Terra, Università di Pisa. MSc thesis.

Wohletz K, Orsi G, De Vita S (1995) Eruptive mechanisms of the Neapolitan Yellow Tuff interpreted from stratigraphic, chemical and granulometric data. J Volcanol Geotherm Res 67:263 – 290.

Figure captions

Figure 1. Shaded relief map (after Tarquini et al. 2007) of the Pozzuoli and Naples bays. Black points represent outcrops surveyed in this work. Dashed ellipse encloses the area which roughly includes the proximal deposits along the crater rims. Red points are the proximal sections used in the deposits description. Key sections of Baia (1) and Fondi di Baia (2 and 3) deposits are also indicated. Dashed black and red lines refer to the inferred CI and NYT caldera borders, respectively.

Figure 2. Pictures of the Baia succession. (a) Opening breccia (Unit I) which overlies the basal paleosoil. (b) Fallout and PDC deposits of Unit II. (c) Detail of a pumice layer shown in (b). (d) PDC layers of the upper part of Unit II. (e) Detail of a breadcrust bomb shown in (d).

(f) Cross-bedding of surge deposits of Unit III. (g) Pumice fallout deposit of Unit II overlying a paleosoil 20 km north of the vent.

Figure 3. Idealized composite stratigraphy of the different phases of the eruption. Analyzed samples and sedimentological data are also reported on the right. The pie charts represent juvenile, lithic and obsidian proportions.

Figure 4. Pictures of the Fondi di Baia succession. (a) Detail of the contact between the fallout phase (Unit II) of the Baia eruption which overlies the basal paleosoil, and the opening breccia of the Fondi di Baia eruption (Unit IV). An oxidation layer separates the two deposits. (b) Detail of the altered, opening breccia of the Fondi di Baia eruption. Outcrop is ~3 m in thickness. (c) PDC deposits of Unit V. Outcrop is ~2.5 m high.

Figure 5. (a) Isopach and (b) isopleth maps of the Baia fallout phase of Unit II. All values are expressed in cm. In the isopleth map, black and white values represent the combination of the five largest clasts and for the 50^{th} percentile of the distribution of the maximum clasts, respectively. Red dots refer to samples used for the reconstruction of the total grain-size distribution.

Figure 6. Total grain-size distribution of Unit II fallout deposits determined by Voronoi tessellation.

Figure 7. (a) to (d) examples of breadcrust, banded bombs from Unit II. (e) and (f) are back-scattered scanning electron microscope images of dense and vesicular, banded juvenile clasts, respectively.

Figure 8. Bulk density (kg/m^3) and vesicularity (vol.%) trends of the representative samples for the different phases of the two eruptive successions. See Table 2 for data.

Figure 9. Bulk density (g cm^{-3}), vesicularity (vol.%), VNDs (cm^{-3}) and decompression rate (MPa s^{-1}) variations for the eruptive succession. Variations in SiO_2, CaO and K_2O (wt%) contents are also given.

Figure 10. Vesicle Volume Distributions (VVDs) plots for modal, low- and high-density fragments analyzed from the samples of the two eruptive successions. See Table S1 for data.

Figure 11. Total alkali vs. silica diagram (TAS, after Le Maitre et al. 1989) with the fields indicating groundmass glass compositions. Baia (white diamonds) and FdB (gray squares) whole rock compositions are also shown.

Figure 12. Schematic model of the eruption. Opening breccia (Unit I), fallout- and PDC- (Unit II) and surge-dominated (Unit III) phases of the Baia event. Opening breccia (Unit IV) of the Fondi di Baia eruption followed by PDC deposits (Unit V) accompanied by ballistic showers of obsidian bombs.

Table 1. Labels, UTM locations, distances from the vent and sedimentological parameters of the samples collected and analyzed in this work. S_{KI} and K_G refer to Skewness and Kurtosis of the grain-size distributions. F1 and F2 are the fractions finer than 1 mm and 63 μm, respectively. For componentry analyses, wt.% of analysed sample is reported.

Table 2. Bulk density (kg/m^3) and vesicularity (vol.%) data of the analyzed samples.

Figure S1. Table showing backscattered images of the MD, LD and HD analyzed clasts from the different samples.

Figure S2. Cumulative Vesicle Size Distribution (CVSD) and cumulative volume fraction plots of the different analyzed samples.

Table S1. Textural parameters of investigated samples from Baia – Fondi di Baia eruptions.

Figure 1

Click here to download Figure Figure 1.tif

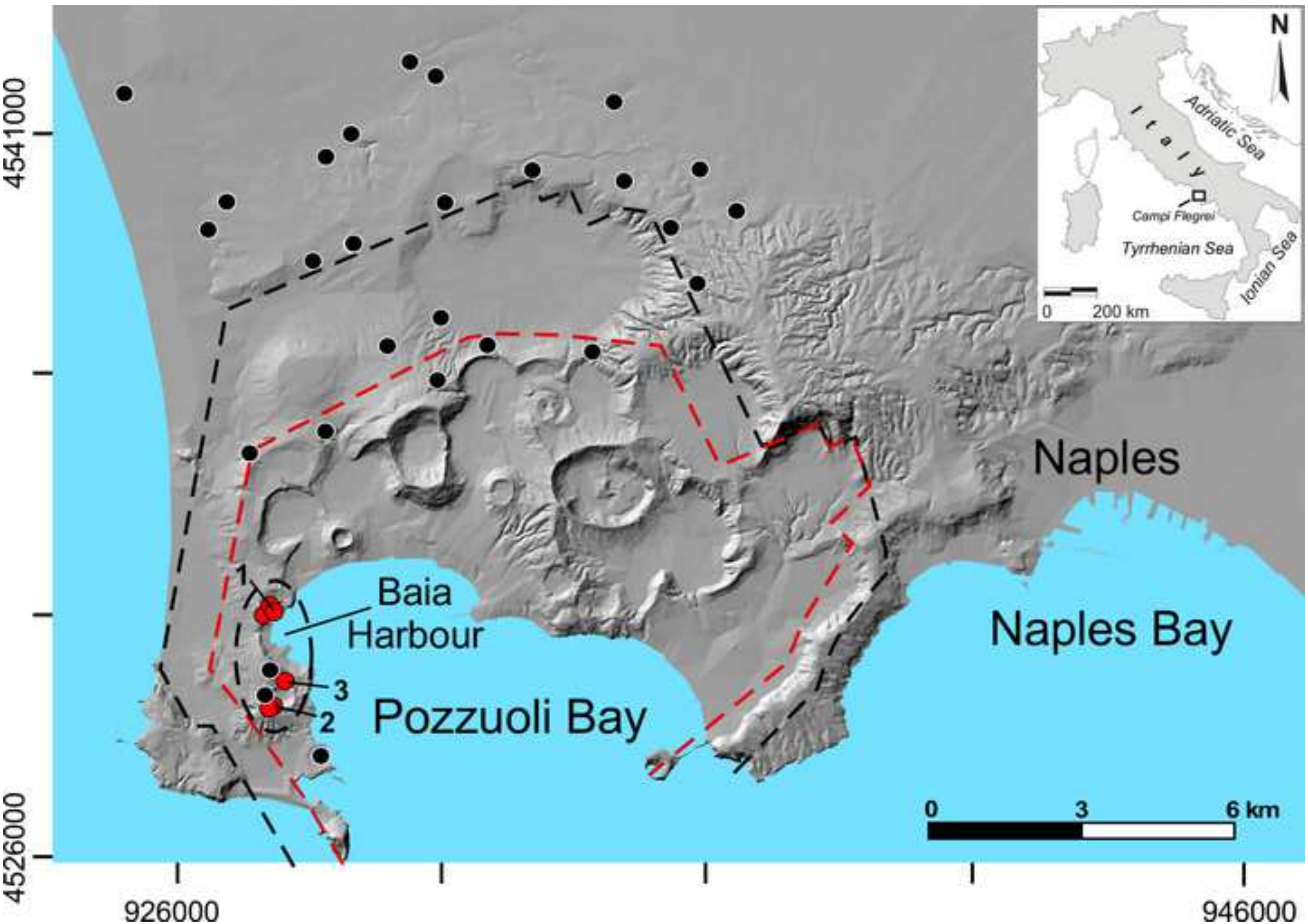

Figure 2 Click here to download Figure Figure 2.tif

Figure 3

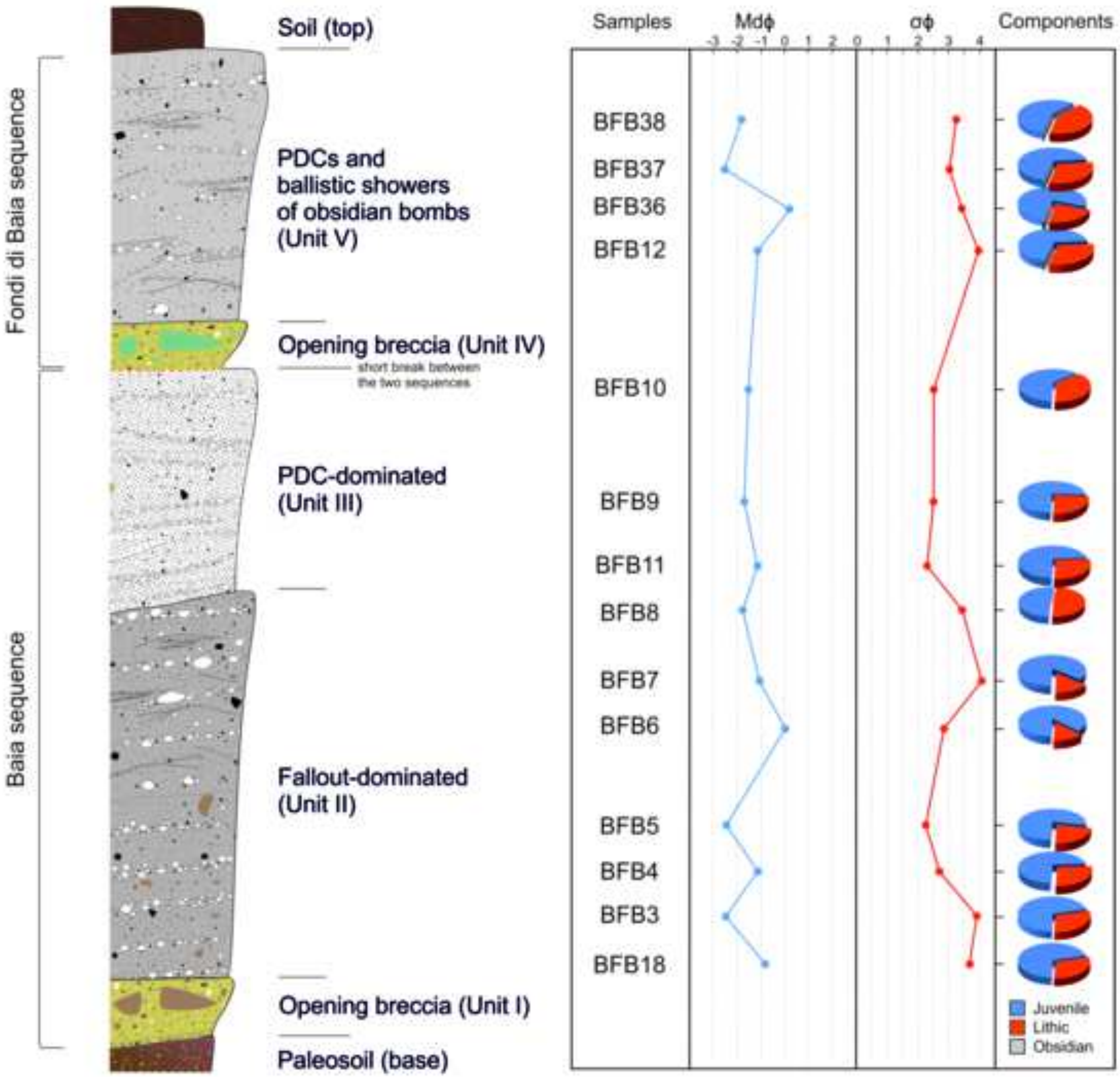

Soil (top)
Fondi di Baia sequence
PDCs and ballistic showers of obsidian bombs (Unit V)
Opening breccia (Unit IV)
short break between the two sequences
Baia sequence
PDC-dominated (Unit III)
Fallout-dominated (Unit II)
Opening breccia (Unit I)
Paleosoil (base)
Samples
Mdϕ
σϕ
Components
BFB38
BFB37
BFB36
BFB12
BFB10
BFB9
BFB11
BFB8
BFB7
BFB6
BFB5
BFB4
BFB3
BFB18
Juvenile
Lithic
Obsidian

Figure 4

Click here to download Figure Figure 4.tif

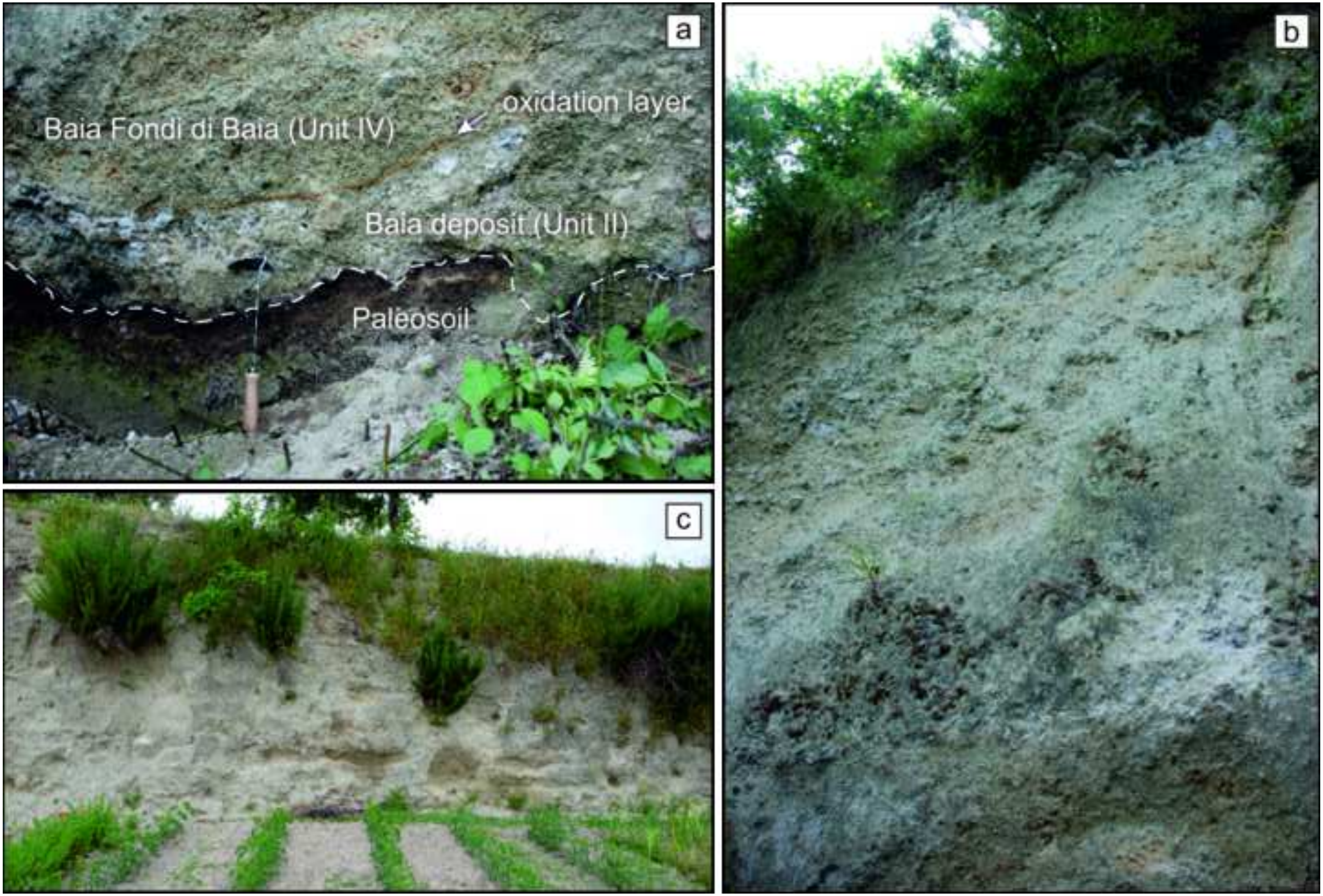

Figure 5

Click here to download Figure Figure 5.tif

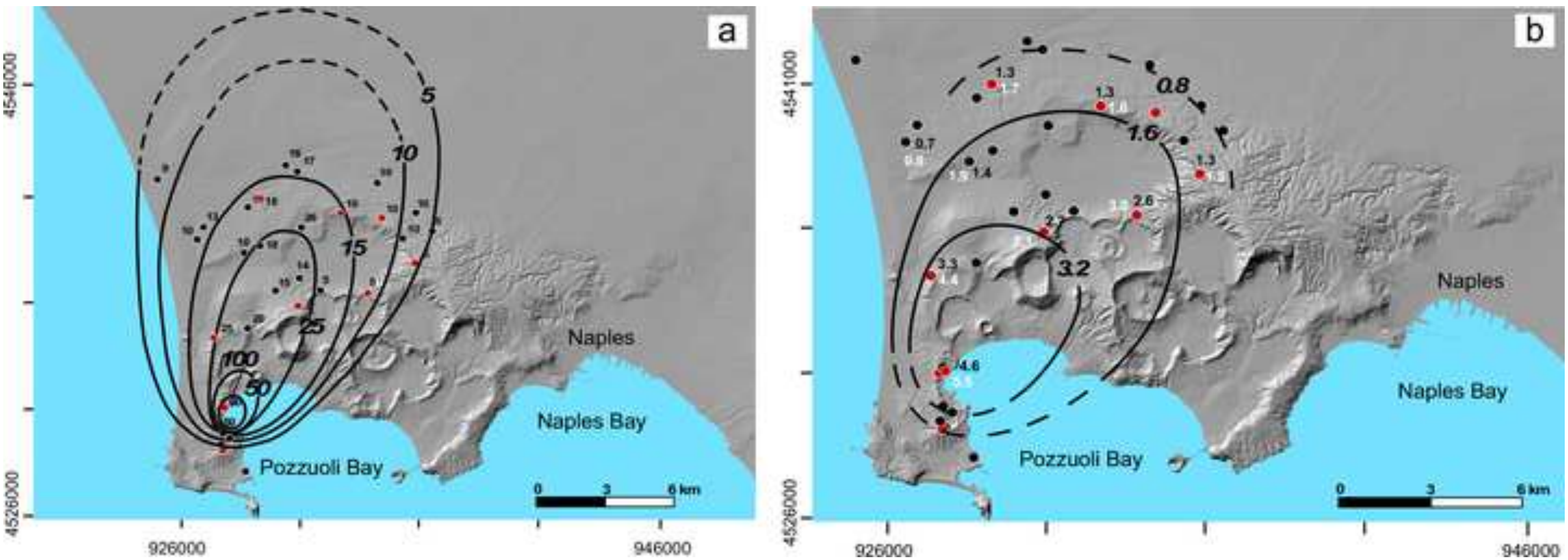

Figure 6

Click here to download Figure Figure 6.tif

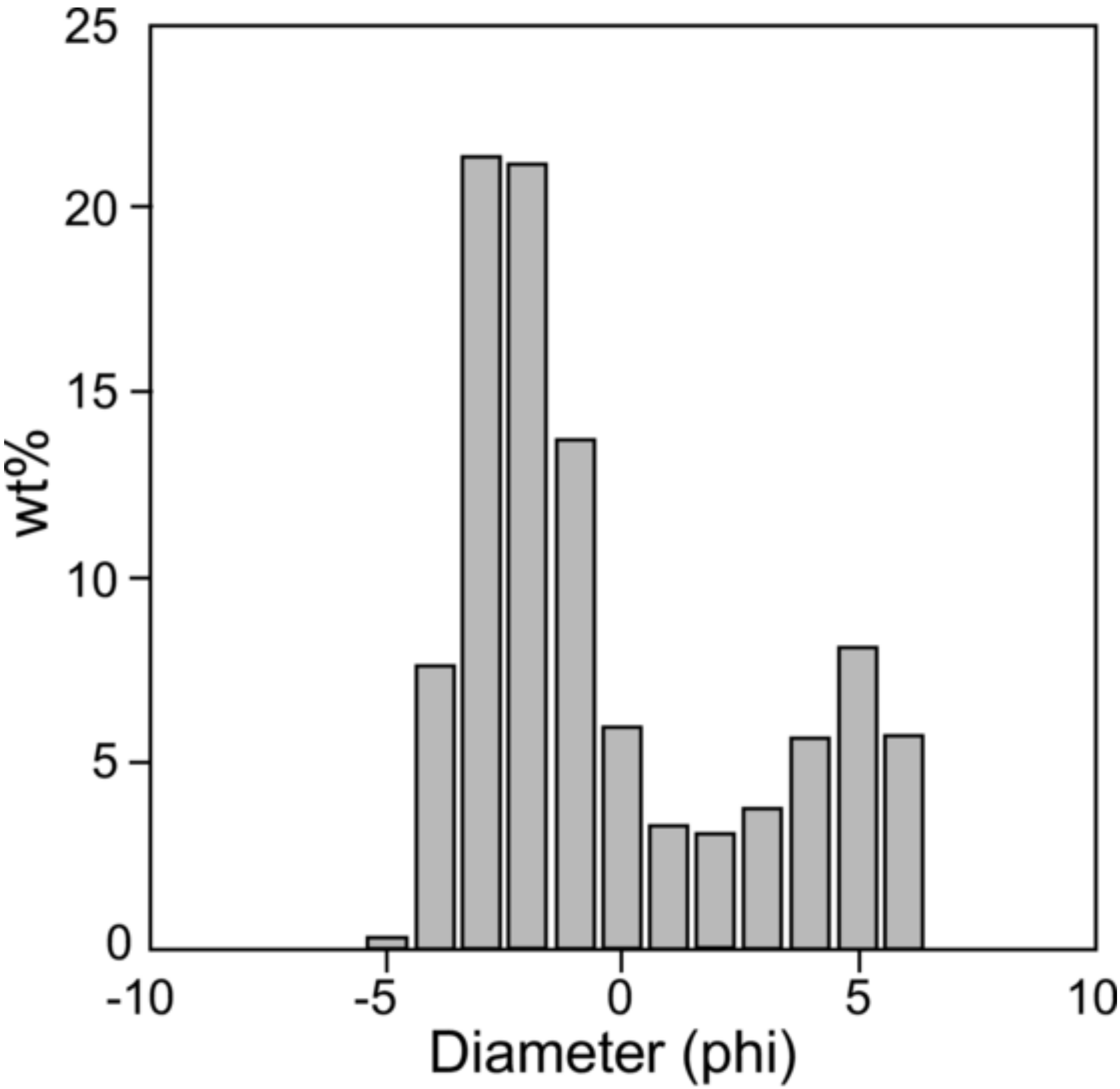

Figure 7

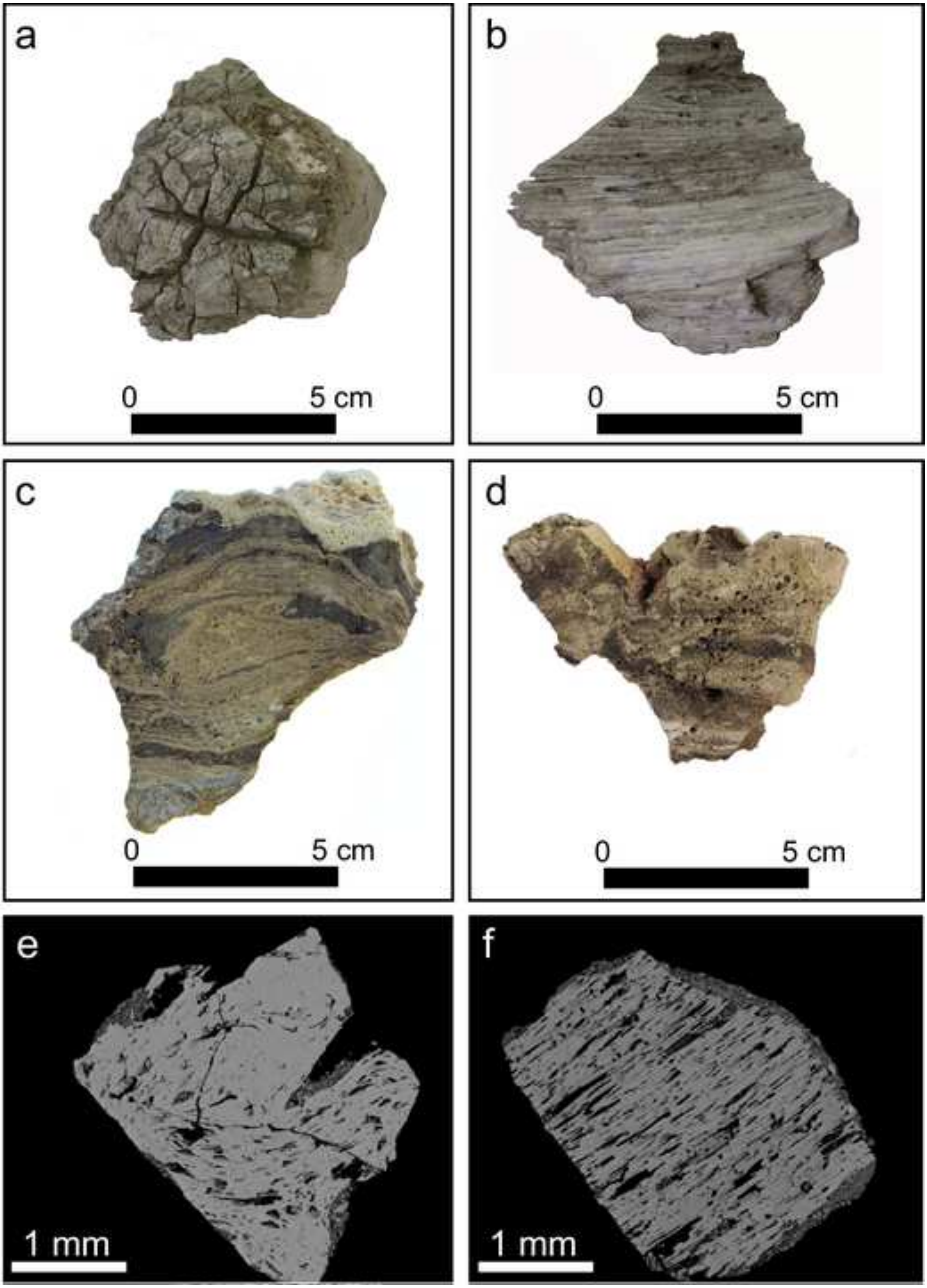

Figure 8

Click here to download Figure Figure 8.tif

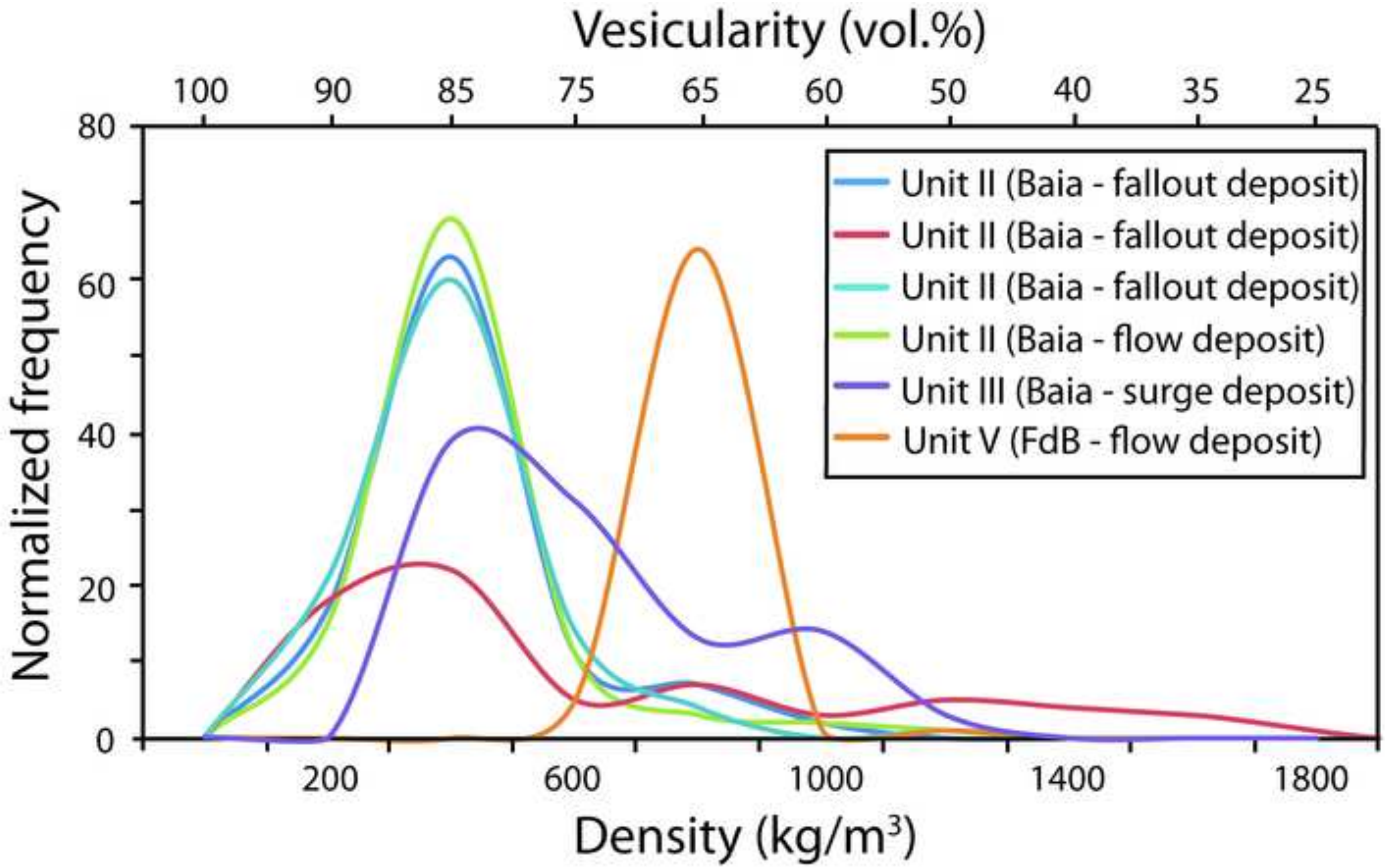

Figure 9

Click here to download Figure Figure 9.tif

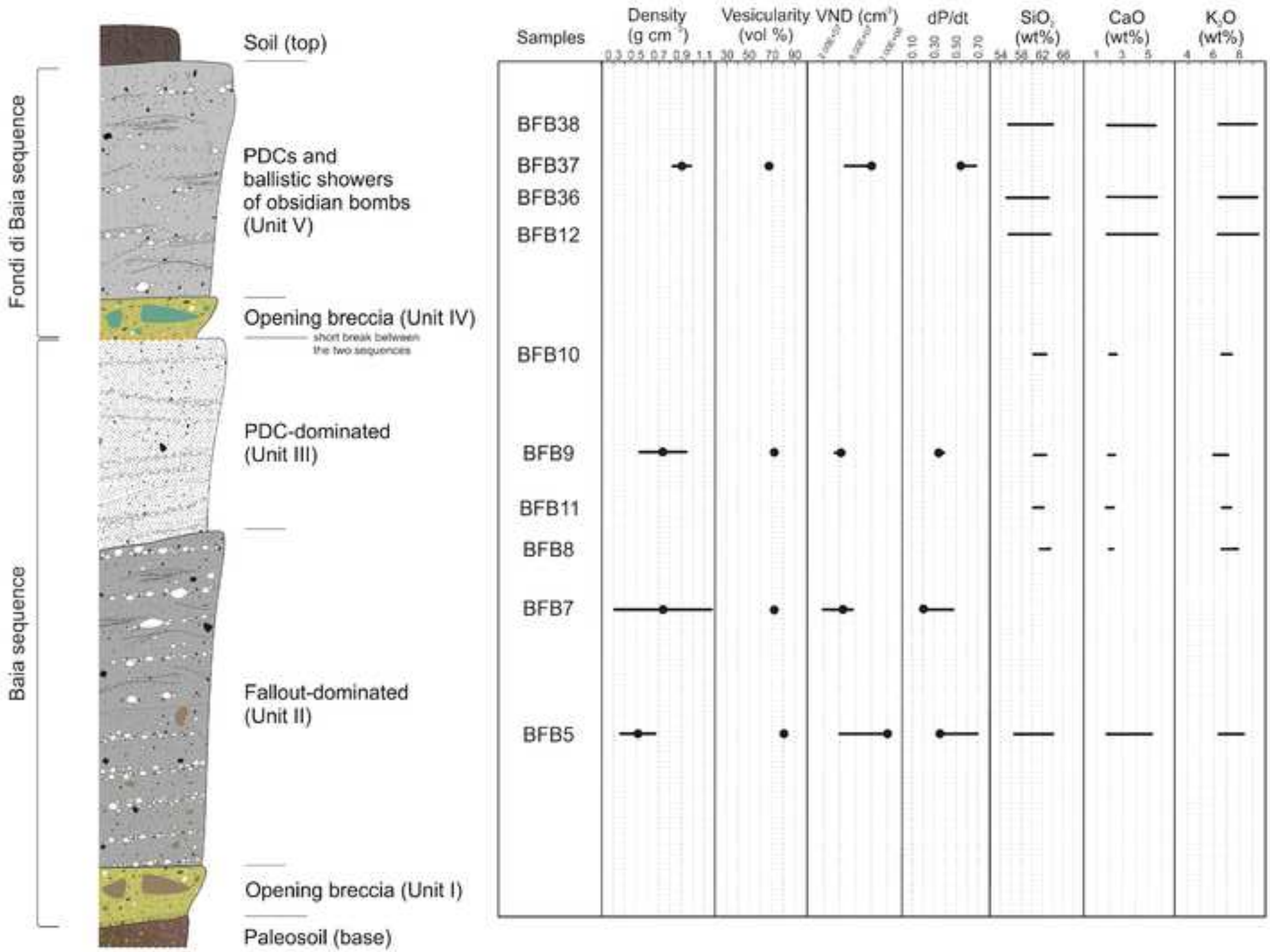

Figure 10

Click here to download Figure Figure 10.tif

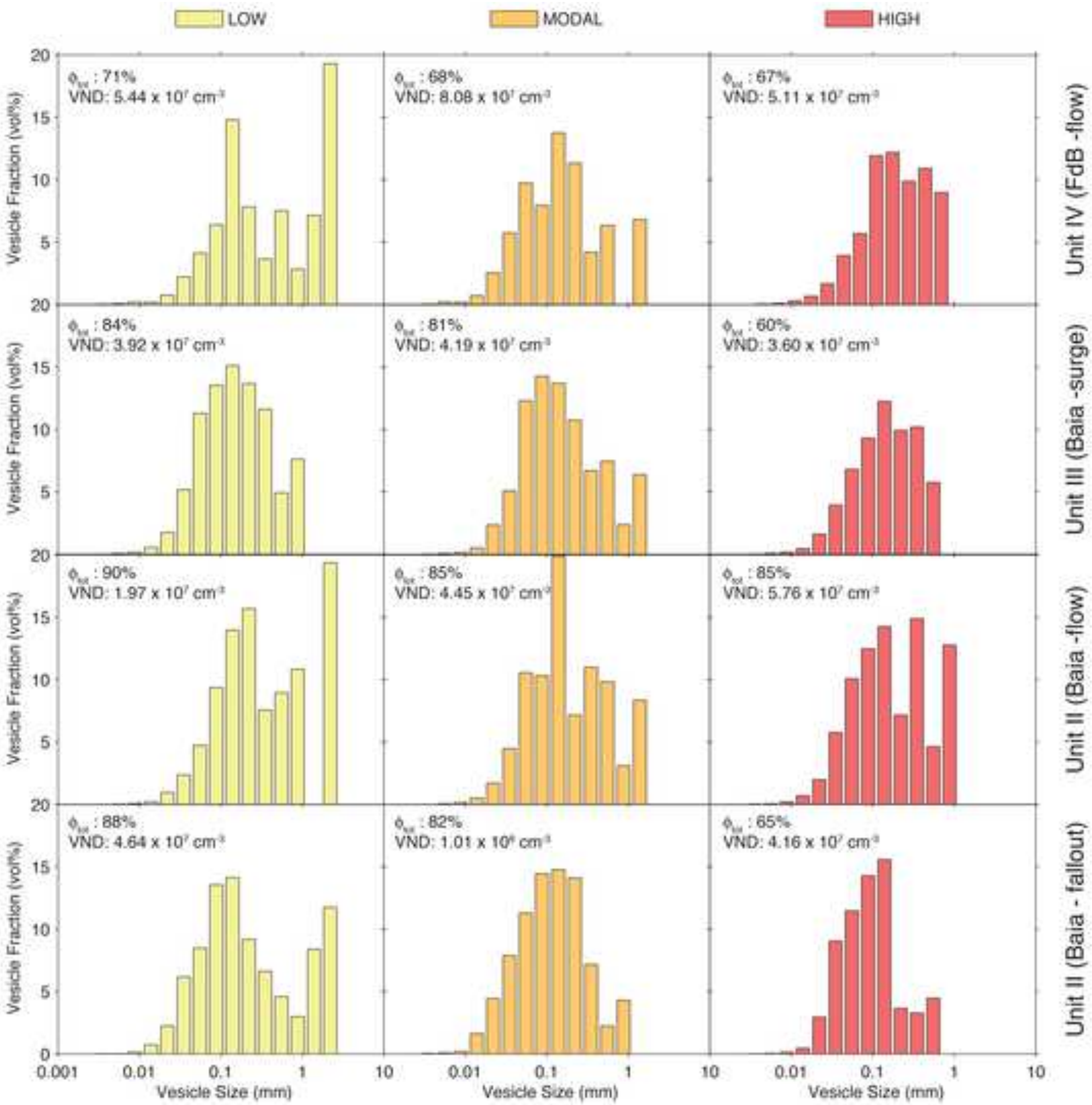

Figure 11

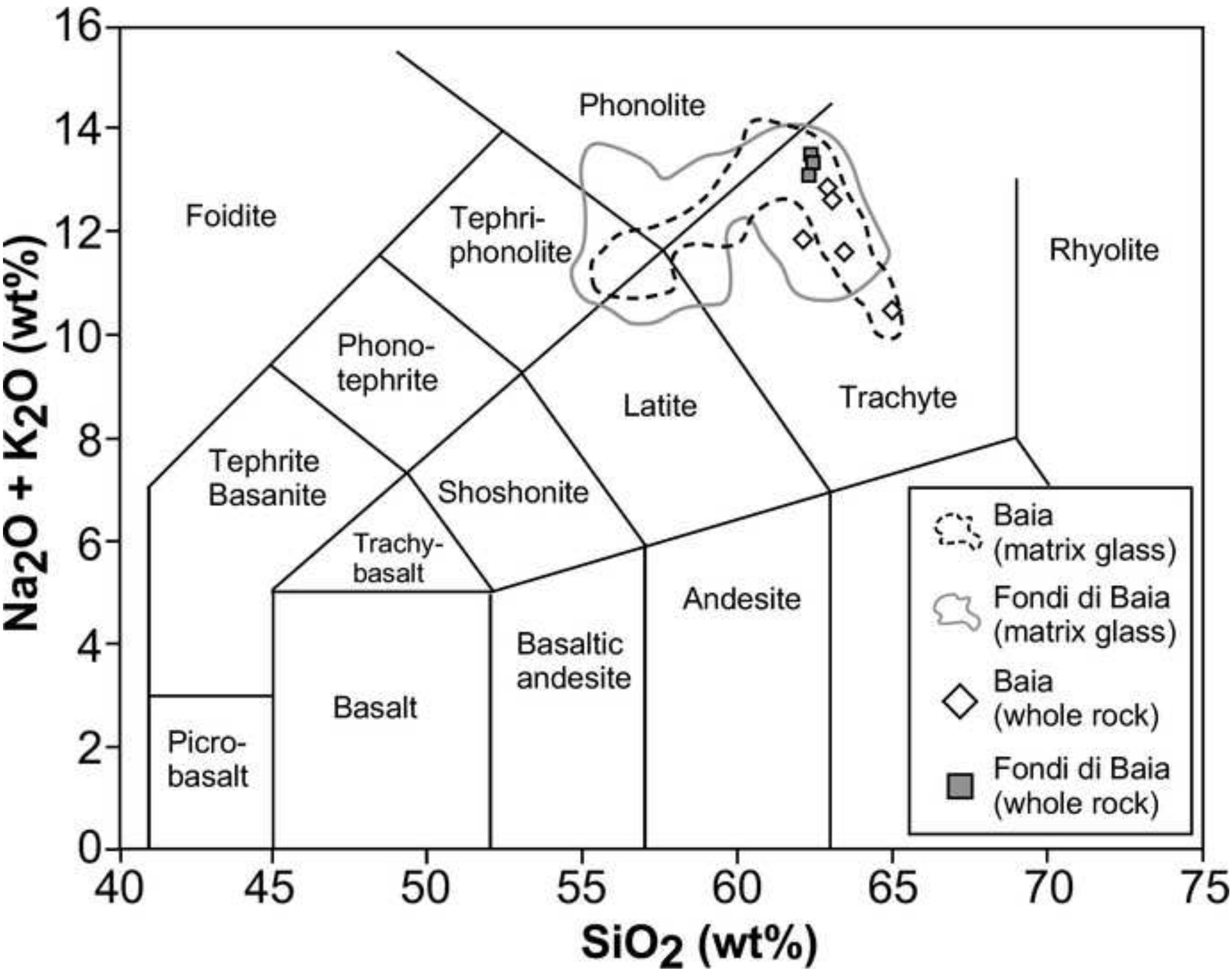

16
14
12
10
8
6
4
2
0
40
45
50
55
60
65
70
75
$Na_2O + K_2O$ (wt%)
SiO_2 (wt%)
Foidite
Phonolite
Tephri-phonolite
Phono-tephrite
Tephrite Basanite
Trachy-basalt
Shoshonite
Latite
Trachyte
Rhyolite
Picro-basalt
Basalt
Basaltic andesite
Andesite
Baia (matrix glass)
Fondi di Baia (matrix glass)
Baia (whole rock)
Fondi di Baia (whole rock)

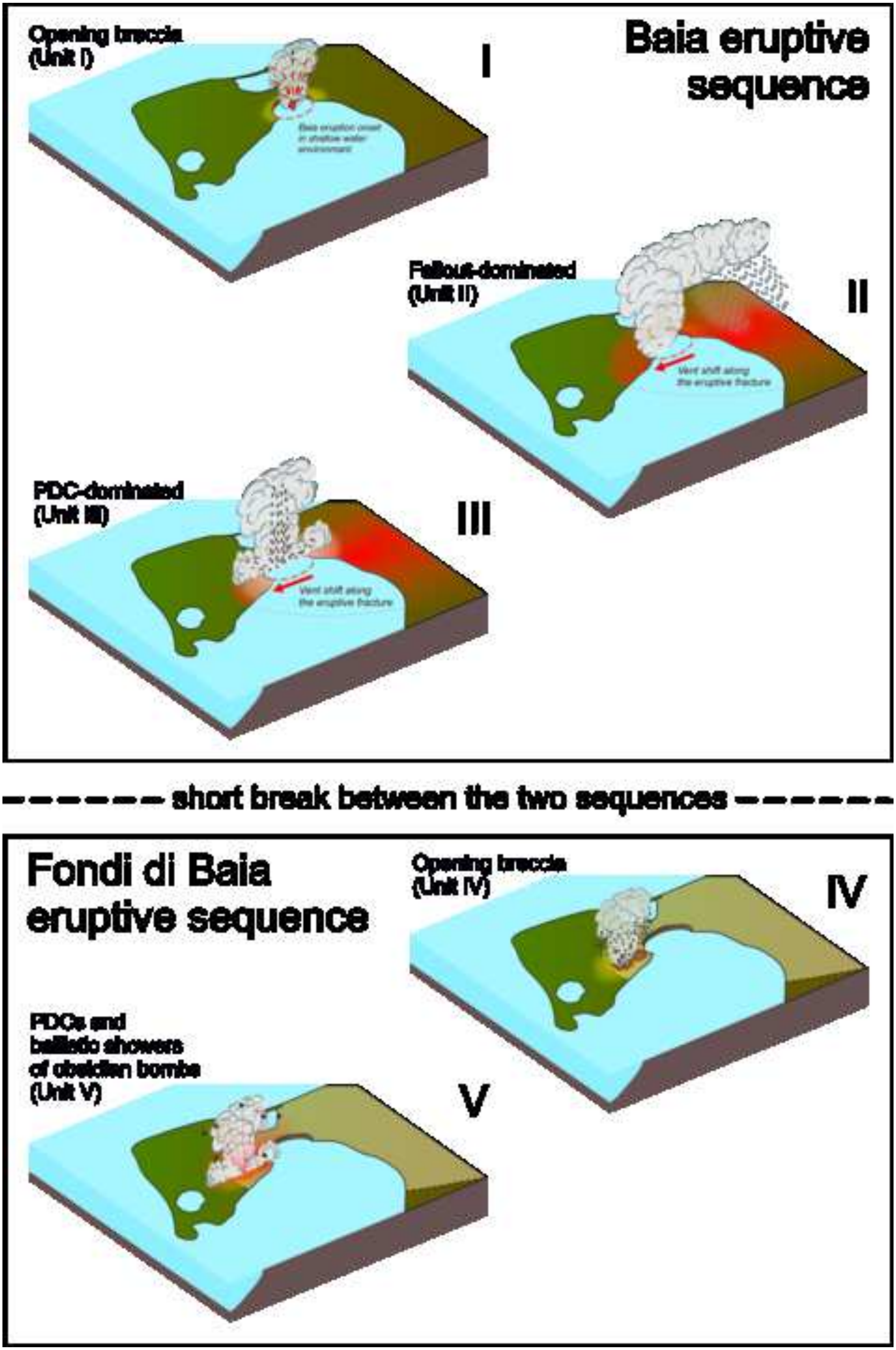
Baia eruptive sequence
Opening breccia (Unit I)
I
Fallout-dominated (Unit II)
II
PDC-dominated (Unit III)
III
short break between the two sequences
Fondi di Baia eruptive sequence
Opening breccia (Unit IV)
IV
PDCs and ballistic showers of obsidian bombs (Unit V)
V

Table 1

Table 1. Labels, locations, distances from the vent and sedimentological parameters of the samples collected and analyzed in this work.

Sample	UTM	Unit	Eruption	Distance km	Md_{Φ}	σ_{Φ}	Sorting	F1	F2	S_{KI}	K_G	Juvenile %	Obsidian %	Lithic %	% analyzed
BFB3	33T 421655 4519327	II	Baia	0.3	-2.47	3.91	Poorly sorted	24.9	11.9	0.5	0.8	50.9	–	49.1	69.8
BFB4	33T 421655 4519327	II	Baia	0.3	-1.12	2.69	Poorly sorted	24.4	6.9	0.3	1.1	77.3	–	26.6	66.5
BFB5	33T 421794 4519371	II	Baia	0.4	-2.45	2.25	Poorly sorted	12.3	5.4	0.4	1.3	77.9	–	22.1	80.5
BFB13	33T 421794 4519371	II	Baia	0.4	-2.33	2.87	Poorly sorted	19.8	7.5	0.5	1.2	77.4	–	22.6	75.3
BFB14	33T 421794 4519371	II	Baia	0.4	2.54	3.11	Poorly sorted	70.2	29.1	-0.1	0.7	86.2	–	13.8	21.7
BFB15	33T 421794 4519371	II	Baia	0.4	1.14	3.80	Poorly sorted	51.3	18.0	-0.0	0.7	91.7	–	8.3	39.3
BFB16	33T 421794 4519371	II	Baia	0.4	-1.61	3.23	Poorly sorted	27.9	10.6	0.4	0.9	90.1	–	9.9	64.7
BFB17	33T 421794 4519371	II	Baia	0.4	-3.13	1.52	Well sorted	9.1	4.2	0.5	2.0	91.9	–	8.1	88.4
BFB18	33T 421794 4519371	II	Baia	0.4	-0.81	3.68	Poorly sorted	31.4	12.6	0.3	0.9	70.3	–	29.7	59.2
BFB6	33T 421794 4519371	II	Baia	0.4	0.03	2.84	Poorly sorted	38.2	6.5	0.2	0.9	87.5	–	12.5	48.6
BFB7	33T 421794 4519371	II	Baia	0.4	-1.06	4.07	Very poorly sor.	30.1	14.9	0.3	0.8	86.0	–	14.0	62.2
BFB8	33T 421794 4519371	II	Baia	0.4	-1.76	3.43	Poorly sorted	25.2	12.6	0.4	0.9	51.5	–	48.5	68.0
BFB9	33T 421762 4519528	III	Baia	0.5	-1.70	2.50	Poorly sorted	16.6	3.4	0.2	1.5	75.1	–	24.9	71.2
BFB10	33T 421762 4519528	III	Baia	0.5	-1.14	2.29	Poorly sorted	19.6	8.2	0.3	1.3	63.1	–	36.9	69.5
BFB11	33T 421762 4519528	III	Baia	0.5	-1.53	2.51	Poorly sorted	18.3	5.0	0.3	1.2	73.4	–	26.6	72.9
BFB12	33T 421780 4517497	V	FdB	1.6	-1.13	3.97	Poorly sorted	30.1	13.0	0.3	0.8	69.8	0.02	30.1	61.0
BFB36	33T 422063 4518067	V	FdB	1.1	0.21	3.42	Poorly sorted	41.9	10.1	0.2	0.8	77.4	1.3	21.3	51.2
BFB37	33T 422063 4518067	V	FdB	1.1	-2.53	3.02	Poorly sorted	19.8	7.0	0.5	1.1	69.1	0.4	30.5	75.1
BFB38	33T 422063 4518067	V	FdB	1.1	-1.80	3.24	Poorly sorted	22.0	6.5	0.3	0.9	58.7	0.3	41.0	71.2
BFB22	33T 421383 4522466	distal	Baia	7	-2.90	1.38	Well sorted	4.0	0.1	0.2	1.2	–	–	–	–
BFB24	33T 425090 4523899	distal	Baia	12	-1.21	4.21	Very poorly sor.	41.6	9.9	0.3	0.6	–	–	–	–
BFB27	33T 428103 4524476	distal	Baia	15	-1.48	3.80	Poorly sorted	37.8	7.1	0.5	0.6	–	–	–	–
BFB29	33T 421836 4517532	distal	Baia	1.7	-1.59	2.80	Poorly sorted	22.6	2.7	0.3	0.9	–	–	–	–
BFB32	33T 430156 4525835	distal	Baia	20	-1.75	3.51	Poorly sorted	29.7	6.1	0.5	0.7	–	–	–	–
BFB34	33T 426939 4528047	distal	Baia	25	-2.46	1.21	Well sorted	7.2	1.2	0.3	1.7	–	–	–	–
BFB39	33T 428747 4527834	distal	Baia	21	1.19	3.56	Poorly sorted	51.2	10.2	-0.0	0.6	–	–	–	–

Table 2

Table 2. Bulk density (kg/m^3) and vesicularity (vol.%) data of the analyzed samples.

Sample	Unit	Eruption (phase)	Density (kg m^{-3})	Standard Deviation	Vesicularity (vol.%)
BFB1	II	Baia (fallout deposit)	530	±160	78
BFB5	II	Baia (fallout deposit)	520	±160	78
BFB17	II	Baia (fallout deposit)	510	±120	79
BFB7	II	Baia (flow deposit)	740	±450	69
BFB9	III	Baia (surge deposit)	740	±220	69
BFB37	V	FdB (flow deposit)	910	±90	62